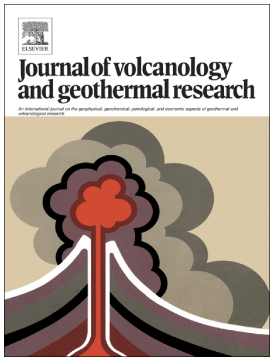

A high resolution 40Ar/39Ar lava chronology and edifice construction history for Tongariro volcano, New Zealand

Leo R. Pure, Graham S. Leonard, Dougal B. Townsend, Colin J.N. Wilson, Andrew T. Calvert, Rosie P. Cole, Chris E. Conway, John A. Gamble, T. 'Bubs' Smith

PII: S0377-0273(20)30108-6

DOI: https://doi.org/10.1016/j.jvolgeores.2020.106993

Reference: VOLGEO 106993

To appear in: *Journal of Volcanology and Geothermal Research*

Received date: 18 February 2020

Revised date: 1 July 2020

Accepted date: 1 July 2020

Please cite this article as: L.R. Pure, G.S. Leonard, D.B. Townsend, et al., A high resolution 40Ar/39Ar lava chronology and edifice construction history for Tongariro volcano, New Zealand, *Journal of Volcanology and Geothermal Research* (2020), https://doi.org/10.1016/j.jvolgeores.2020.106993

A high resolution $^{40}Ar/^{39}Ar$ lava chronology and edifice construction history for Tongariro volcano, New Zealand

Leo R. Pure[a], Graham S. Leonard[b], Dougal B. Townsend[b], Colin J. N. Wilson[a], Andrew T. Calvert[c], Rosie P. Cole[d], Chris E. Conway[e], John A. Gamble[a,f], T. 'Bubs' Smith[g]

[a] School of Geography, Environment and Earth Sciences, Victoria University of Wellington, PO Box 600, Wellington 6140, New Zealand

[b] GNS Science, Avalon Research Centre, PO Box 30368, Lower Hutt 5010, New Zealand

[c] US Geological Survey, 345 Middlefield Road, MS-937, Menlo Park, CA 94025, USA

[d] Department of Geology, University of Otago, PO Box 56, Dunedin 9054, New Zealand

[e] Geological Survey of Japan, AIST, 1-1-1 Higashi, Tsukuba, Ibaraki 305-8567, Japan

[f] School of Biological, Earth and Environmental Sciences, University College Cork, Eire

[g] Ngati Tūwharetoa, Turangi, New Zealand

Keywords: Tongariro, Ar/Ar dating, Eruptive history, Composite volcano, Glaciovolcanism, Andesite volcanism

Manuscript for *Journal of Volcanology and Geothermal Research*
Revised version (LRP edited) to co-authors: 18 February 2020

corresponding author: leo.r.pure@tutamail.com

Abstract

Detailed mapping and geochronological investigations of edifice-forming materials reconstruct the growth history of Tongariro volcano, New Zealand, and subdivide the edifice into thirty six distinct units which are organised into twelve formations and constituent members. Twenty nine new $^{40}Ar/^{39}Ar$ age determinations, along with published K/Ar ages combined with volume estimates, petrographic observations and rock chemistry provide an integrated history of the volcano's growth through edifice-forming lavas and pyroclastic deposits. The oldest lava (512 ± 59 ka, 2 s.d.) is a small inlier of basaltic-andesite on Tongariro's NW sector that may reflect a nearly buried independent volcano. The next oldest material that can be confidently attributed to a Tongariro source is 304 ± 11 ka andesite, incorporated as boulders in late Pleistocene ejecta from the Tama Lakes area. In-situ lavas at Tongariro date from 230 ka to present, including numerous flows erupted during glacial periods and building the edifice unevenly due to emplacement against valley-filling ice bodies. Tongariro has a total edifice volume of ~90 km^3, 19 km^3 of which is represented by exposed map units, with glacial deposits amounting to <1 km^3. The ring plain volume immediately adjacent to the volcano contains ~60 km^3 of material.

Sequential eruptive records, from 230 ka to present, reveal an irregular cyclicity in MgO concentrations over ~10-70 kyr intervals. During these cycles, rapid (≤10 kyr) increases in MgO concentrations to ≥5-9 wt% are inferred to reflect episodes of enhanced mafic magma replenishment, with maxima at ~230, ~160, ~117, ~88, ~56, ~35, ~17.5 ka and during the Holocene, which are each followed by gradual declines to ~2-5 wt%. Field evidence, including extensive moraines and U-shaped valleys, and lava textures, implies repeated occupation of valleys on Tongariro by major glaciers and possibly ice caps. During periods of major ice coverage, which generally correlate with global cold climate/glacial Marine Isotope Stages, edifice-building rates on Tongariro were only 17-26 % of those during warmer climatic periods. Because the changes in edifice-building rates do not coincide with changes in the magmatic system, these contrasts are inferred to reflect a preservation bias whereby materials erupted onto ice were contemporaneously (or subsequently, as ice masses melted) conveyed to the ring plain as debris rather than building the edifice. Although the Tongariro edifice is smaller than that of neighbouring Ruapehu (~150 km^3), the exposed edifice materials on Tongariro record a longer and more complex growth history. The wider geographic distribution of <50 ka vent locations at Tongariro reflects greater rifting rates than at Ruapehu.

1. Introduction

The archetypical surficial expressions of arc magmatism are large (tens to hundreds of cubic kilometres) composite stratovolcanoes (Gill, 1981; Davidson and de Silva, 2000). The temporal, spatial and compositional records of how stratovolcanoes grow provide insights into arc magmatic processes on scales of 10^4-10^5 years or more. The keys to interrogating these records exist within detailed sampling of edifice-forming eruptives and mapping them into either compositionally related or distinct units, coupled with accurate age determinations to quantify stratigraphic ordering. With stratovolcanoes, such studies most often utilise $^{40}Ar/^{39}Ar$ geochronology on lavas (e.g. Dungan et al., 2001; Gamble et al., 2003; Fierstein et al., 2011; Conway et al., 2016), which are generally the best-preserved volcanic products on stratovolcano edifices (e.g. Singer et al., 1997; Hildreth and Fierstein, 2012; Sisson et al., 2014). Pyroclastic deposits are vulnerable to erosion on the edifice itself and tend to weather rapidly during soil formation at lower elevations. Because of these factors, records of pre-Holocene explosive eruptions from stratovolcanoes are patchy and biased towards preserving evidence of larger events ($\geq$1 km^3: e.g. Watt et al., 2013; Weller et al., 2015).

In addition, the presence or absence of glacial ice has a fundamental control on the emplacement behaviour and preservation potential of erupted materials at stratovolcanoes (e.g. Mathews, 1952; Lescinsky and Sisson, 1998; Conway et al., 2015). Lescinsky and Sisson (1998) report examples of Pleistocene lavas on Mount Rainier that did not flow onto valley floors because the valleys were occupied by glaciers. Hildreth and Fierstein (2012) report rare ponds of welded ignimbrite erupted from Katmai volcano that were emplaced over glaciers at ~23 ka, during the coldest part of the Last Glaciation, and are not preserved where ice existed at that time. Hildreth (1996) documented an intracaldera tuff at Kulshan caldera: the only other known products of this event are tephra deposits preserved 200 km from source and it is inferred that ice coverage precluded the in-situ preservation of other proximal (but extra-caldera) eruption products. Lava emplacement over snow has been observed historically at Tolbachik volcano where the likelihood of preservation is related to whether lavas burrow down to bedrock or remain above ice masses (Edwards et al., 2015). At times of significant ice coverage, the latter is evidently more likely (e.g. Lescinsky and Sisson, 1998).

This study presents new field mapping, along with new $^{40}Ar/^{39}Ar$ geochronology and selected geochemical data, to establish an eruptive chronology for edifice-forming products and peripheral vents of Tongariro volcano, New Zealand. In particular, these data are used to address the following questions that arise from studies of this and other mid- to high-latitude volcanoes that have been subjected to glaciation.

- Are there biases in exposure and/or preservation in volcanic materials on stratovolcano edifices that relate to various degrees of ice coverage during glacial/interglacial cycles?
- Are valleys cutting into previously glaciated Quaternary stratovolcanoes primarily erosional, or could they reflect landforms produced by the preferential emplacement of lava along the ridges between glaciated valleys?
- Does deglaciation cause an increase in eruption rates at stratovolcanoes due to edifice unloading and magma system depressurisation?

Interactions between ice and volcanism have been previously recognised at Tongariro and neighbouring Ruapehu volcano (Conway et al., 2015, 2016; Townsend et al., 2017; Cole et al., 2018). Tongariro displays evidence for extensive Quaternary glaciation in the form of moraines (Eaves et al., 2016a) and lava-ice interaction textures (Cole et al., 2018). However, the degree to which glaciation has affected preserved volumes and edifice growth styles has not yet been quantified on Tongariro. As a counterpoint to the potential for interaction with glacial ice, an alternative view has been that glaciated stratovolcanoes grow as symmetrical cones during bursts of eruptive activity (like Tongariro's Ngauruhoe cone in the present context) and are subsequently scoured by glaciers to produce valleys (Hobden et al., 1996; Singer et al., 1997, 2008; Dungan et al., 2001) and "ice-ravaged" landforms (Hildreth and Lanphere, 1994). However, accumulating evidence for lava-ice interactions at many stratovolcanoes favours syn-glacial edifice growth models (e.g. Lescinsky and Sisson, 1998; Conway et al., 2016; Cole et al., 2018, 2019), which interpret valleys as primarily constructional landforms where the valley walls and ridgetops are built up around valley-filling ice masses. Such growth patterns can explain how some unusual and asymmetric landforms develop in upper edifice regions, without needing to invoke caldera or sector collapses. Some workers have proposed that eruptive rates at stratovolcanoes increase following deglaciation due to depressurisation of the magma system (Jicha et al., 2012; Rawson et al., 2016), whereas others show that peak eruptive rates occurred within glacial periods (e.g. Calvert et al., 2018).

Previous mapping at Tongariro by Gregg (1960), Lee et al. (2011) and I.A. Nairn (unpublished mapping) has been assembled and reinterpreted by Townsend et al. (2017); that work led to identifying gaps in our understanding and directing where new work could be undertaken (e.g., this study). Previous geochronological and geochemical studies by Hobden et al. (1996) and Hobden (1997), respectively, built on earlier work by Topping (1974), Cole (1978) and Wahyudin (1993). Other areally limited studies include Hobden et al. (2002) on Ngauruhoe and Cole et al. (2018) on parts of Tongariro. Building on these datasets, the current study presents a suite of new mapping observations, plus geochronological and selected geochemical

data that are used to revise the work in Townsend et al. (2017) and provide a comprehensive picture of the growth of a typical arc stratovolcano.

2. Geological setting of Tongariro volcano

Tongariro volcano is located in the andesite-dominated southern Taupō Volcanic Zone (TVZ) in the North Island of New Zealand (Wilson et al., 1995). The TVZ is an actively rifting continental volcanic arc fuelled by the westward subduction of the Pacific Plate beneath the Indo-Australian Plate, with a convergence rate of ~43 mm/yr at the latitude of the central and southern TVZ (Nicol et al., 2007). Active extension is greatest (~15 mm/yr) in the northern TVZ arc at the Bay of Plenty coast and decreases to ~7 mm/yr at the latitude of Tongariro (Wallace et al., 2004; Beavan et al., 2016; Gómez-Vasconcelos et al., 2017; Villamor et al., 2017); rifting terminates ~40 km south of Tongariro (Fig. 1; Wallace et al., 2004; Villamor and Berryman, 2006).

Both Tongariro and Ruapehu occupy an active graben between uplifted eastern (Kaimanawa Mountains) and western shoulders that are underlain by Mesozoic greywacke. Despite evidence for previous and ongoing extension (Wallace et al., 2004; Villamor and Berryman, 2006; Jiao et al., 2014; Beavan et al., 2016), it is unclear whether rifting-related subsidence in the southern TVZ has significantly lowered the summit elevations of Tongariro or Ruapehu, and affected the potential to generate and retain significant ice masses on these volcanoes during glacial periods. Tongariro and Ruapehu are the only stratovolcanoes in New Zealand that have supported substantial glaciers repeatedly over their lifespans (e.g. McArthur and Shepherd, 1990). Glacial deposits are preserved at both volcanoes for at least three periods of major glacial advance in their 200-300 kyr histories (Conway et al., 2015; Eaves et al., 2016a; Townsend et al., 2017). Tongariro has also undergone more intense faulting of similar-age materials than at Ruapehu (Fig. 1), which has lowered the central edifice area relative to the flanks (Gómez-Vasconcelos et al., 2017).

Tongariro's composite edifice is constructed from volcanic products erupted from multiple vents (Gregg, 1960; Cole, 1978; Hobden et al., 1996; Townsend et al., 2017; Cole et al., 2018). Younger vents, such as those forming the cones of Ngauruhoe and Red Crater, are obvious from their prominence in the landscape and the presence of lava flows that can be traced back to their source (Fig. 2). However, older vent locations (>50 ka) are less clear because of burial by younger eruptives or sediments or can only be inferred from material preserved elsewhere such as on the ring plain. The oldest products that are directly (physically) linked with their vent are those sourced from North Crater (Fig. 2) between 45 and 36 ka.

3. Eruptive stratigraphy of Tongariro

3.1. Introduction

The mapping reported here subdivides Tongariro's edifice-forming materials into twelve formations (including five newly defined), some of which are subdivided into members. All the units are formally defined and their dating constraints explained in the Supplementary Materials. Collectively, these formations and members form thirty five distinct, edifice-forming stratigraphic units (excluding some undifferentiated eruptives and also the Te Whaiau Formation, which probably represents a sector collapse of north-western Tongariro). This breakdown is comparable with the four formations and constituent members that collectively form twenty two distinct edifice-forming units on nearby Ruapehu (Hackett and Houghton, 1989; Conway, 2016; Conway et al., 2016; Townsend et al., 2017).

Like Ruapehu, map units for Tongariro are jointly defined by a combination of field relations, geochronological data, sample petrography, geochemistry, spatial distributions and lithological characteristics (see Supplementary Materials). Regarding spatial distinctions, vent areas are defined as having a ≤1 km diameter, whereas if vent areas are separated by ≥2 km, they are considered as being distinct. The naming conventions used here are consistent with recent geological mapping at Ruapehu; formations and members are named after nearby landmarks, flora or fauna in the Māori language.

3.2. Systematic descriptions of stratigraphic units

The age ranges specified in the titles of map units described systematically below reflect adopted ages derived from joint consideration of both field relationships and geochronological data (see Supplementary Materials section S5 for details). Formations are abbreviated with uppercase two-letter codes. Members are abbreviated with lowercase three-letter codes, where the first letter denotes the most distinctive composition (e.g. Fierstein et al., 2011): m = basaltic-andesite, a = andesite, d = dacite. No basalts or rhyolites have been found at Tongariro.

This study contributes a total of 29 new $^{40}Ar/^{39}Ar$ age determinations (Table 1) that are integrated with previous K/Ar age determinations by Stipp (1969) and Hobden et al. (1996) for each map unit and summarised in Fig. 3 (see also Supplementary Materials section S5). Where included, radiocarbon ages are stated as calibrated ages to be consistent with other radiometric age data. All radiometric age results are cited with 2 s.d. analytical uncertainties.

Petrographic observations, SiO_2 and MgO concentrations, and unit lithologies are summarised for each map unit in Table 2. Major oxide (and Sr and Ba) concentrations are

reported for representative samples in Table 3 and the full dataset is presented in the Supplementary Materials. New petrographic observations and major oxide concentrations are supplemented with data from Cole (1978, 1979), Wahyudin (1993), Hobden (1997), Cole et al. (2018), D. B. Townsend and G. S. Leonard (unpubl. data, 2019) and a small number of XRF analyses in GNS PETLAB from pre-1980 investigations.

3.2.1. Otamatereinga Formation (512 ± 59 ka) – OT

An inlier of basaltic-andesite lava on Tongariro's western flank (Fig. 4) is the oldest dated material on Tongariro (512 ± 59 ka: Table 1), but probably represents an older edifice, comparable to Maungaku or Maungakatote volcanoes to northwest of Tongariro (Fig. 1), that is almost entirely buried.

3.2.2. Tupuna Formation (between 349 and 293 ka) – TU

The Tupuna Formation is not found in-situ. It is represented by fragments of hornblende-phyric andesite up to 0.4 m across, found predominantly eastwards of and up to ~3 km from Lower Tama lake (Fig. 4: Hobden, 1997; Nairn et al., 1998), matching the dispersal of juvenile material in the ~11 ka Wharepu eruption deposit (unit PM5 of Nairn et al., 1998; Heinrich et al., 2020). This association suggests that Tupuna Formation clasts represent a lava flow or flows that were excavated as accidental lithics from beneath the Lower Tama Lake area (Fig. 4). An age determination on a Tupuna Formation boulder of 304 ± 11 ka (Table 1: LP113) has mixed agreement with previous K/Ar age determinations of 266 ± 6 ka (sample 3254: Hobden et al., 1996 after Stipp, 1969) and 273 ± 44 ka (TG136: Hobden et al., 1996). The compositions and mineralogy of Tupuna Formation andesites are similar to those of andesite boulders in the 349-309 ka (Pillans, 1983; Downs et al., 2014) Turakina Formation debris flows (Tost and Cronin, 2015), reported from a location ~100 km SW of Tongariro in the Whanganui Basin.

3.2.3. Haumata Formation (between 290 and 189 ka) – HA

The Haumata Formation, consisting of lavas and minor pumiceous ignimbrite erupted between 290 and 189 ka, is divided into seven members, plus an eighth undifferentiated unit that is a poorly exposed, landscape-forming unit in the upper NE Oturere valley (Fig. 4). Spatial overlap with published map units is summarised in Supplementary Materials section S5. Haumata Formation eruptives are characterised by Fe-Ti oxide pseudomorphs after amphibole (1-5 vol%) that are more abundant than in other Tongariro eruptives (always ≤1 vol%). Haumata

Formation eruptives are primarily exposed in the southern portion of Tongariro's edifice where they radiate clockwise SE to W and dip 10-25 ° away from a source vent area under the Holocene Ngauruhoe cone, except for the Waipoa Member (Figs. 4, 5: Moebis et al., 2011; Townsend et al., 2017). Lavas from the 195-189 ka Waipoa Member dip E-ESE 10-20 ° away from present-day Central Crater (Fig. 2), which was probably the source vent area (Fig. 4).

Lower Tama Member (alt: between 290 and 242 ka). This member consists of low-K_2O andesite lavas exposed exclusively in ~100 m thick sections on the ridge east of Lower Tama lake, within ~1 km of the lake itself (Fig. 4). The lavas contain abundant Fe-Ti oxide pseudomorphs after amphibole (denoted hb-ox in Table 2), which suggest similar magmatic histories and possibly a shared magma system with the Tupuna Formation.

Tutangatahiro Member (mtu: between 229 and 220 ka). Basaltic-andesite lavas of the Tutangatahiro Member are exposed in the SW and NE walls of Waihohonu valley and at the valley head as an inlier at 1500 m a.s.l. on the Ngauruhoe cone (Fig. 4). No lower contact is observed (Fig. 3). At least seven flows form a conformable succession, collectively up to 150 m thick with individual flow thicknesses that are typically 20 m. The farthest-travelled flow is exposed on State Highway 1, ~10 km from the inferred vent location now beneath Ngauruhoe.

Tawhairauiki Member (atw: between 220 and 214 ka). This member comprises at least four conformable, ridge-forming andesite lavas, collectively ~60 m thick and overlying Tutangatahiro Member lavas in the NE Waihohonu valley (Fig. 4). Runout distances are up to 9 km from the inferred vent beneath Ngauruhoe (Fig. 4). Tawhairauiki Member lavas contain Fe-Ti oxide pseudomorphs after amphibole, but they are less abundant (≤2 vol%) than in other ≥190 ka lavas. However, their presence indicates a similar magmatic history and possibly a shared magma system with eruptives of the Haumata and Tupuna formations.

Upper Tama Member (aut: between 214 and 207 ka). The Upper Tama Member is composed of andesite lavas and minor volumes of pumiceous ignimbrite near Upper Tama Lake (Figs. 4, 5), which form the basal halves (~60 m) of bluffs surrounding the lake. At the Tama-trig ridgeline, ~1.5 km east of Upper Tama lake, a sequence of ~20 m-thick lavas capping ~50 m of pyroclastic deposits occurs and, southwards, these lavas thicken to ~200 m suggesting lateral impoundment by ice (Hobden, 1997; Townsend et al., 2017). The pumice-rich ignimbrite material is preserved only where capped by lava.

Toatoa Member (ato: between 207 and 200 ka). Toatoa Member andesite lavas overlie the Tawhairauiki and Upper Tama members on Tongariro's southern flank (Figs. 3, 4, 5). Toatoa Member lava also forms a ≥100 m thick unit with a rubbly upper surface and no apparent

interior layering in the basal bluffs of Pukekaikiore. Toatoa Member andesites also contain Fe-Ti oxide pseudomorphs after amphibole, as with other Haumata Formation eruptives.

Pukekaikiore Member (apk: between 200 and 190 ka). Pukekaikiore Member corresponds to a ~100 m-thick andesite lava flow that forms the upper bluffs on the northern side of Pukekaikiore (Figs. 4, 6). The inferred vent location is now buried beneath Ngauruhoe. The Toatoa and Pukekaikiore members together form the 'old' Pukekaikiore eruptives of Patterson and Graham (1988) and Hobden (1997), as distinct from the definitions adopted here.

Waipoa Member (awp: between 195 and 189 ka). Waipoa Member andesite lavas are the oldest Tongariro eruptives that, based on their distribution, were erupted from an area near present-day Central Crater (Figs. 3, 4). Up to five conformable lavas, totalling up to 100 m in thickness, are best exposed on the NE Oturere valley wall, but the basal contact is not observed. Ages suggest that the Waipoa and Pukekaikiore members may have erupted contemporaneously, but there are no field contacts to confirm this (Fig. 3). Distributions of these two members indicate a shift in vent focus from the southern edifice (Pukekaikiore Member) to the northern edifice (Waipoa Member) (Figs. 3, 4), albeit with eruption of magmas with similar compositions (Tables 2, 3).

3.2.4. Mangahouhounui Formation (between 189 and 130 ka) – MH

Mangahouhounui Formation products (except for the Tātaramoa Member) erupted from a vent area in the present-day position of Central Crater (Figs. 3, 4). These lavas, agglutinates and breccias dip 10-20 ° away from Central Crater in N, NE, E and SE directions and are mainly exposed in the Mangahouhounui valley, although minor volumes also occur elsewhere (Fig. 4). The name of the formation is retained from previous usage (e.g. Townsend et al., 2017); however, its mapped distribution and subdivision into members is revised. Large plagioclase and clinopyroxene phenocrysts up to 9 mm long distinguish Mangahouhounui Formation eruptives from other Tongariro volcanic products, in which those crystals are ≤5 mm (Table 2).

Te Pakiraki Member (dpk: between 189 and 130 ka). Up to 20 lava flows, agglutinate units and intercalated lapilli tuff breccias exposed in the Mangahouhounui valley and distal SW Oturere valley constitute the Te Pakiraki Member (Figs. 4, 7). Compositions are mostly high-silica andesite but range from basaltic-andesite to dacite (Tables 2, 3). Large plagioclase (up to 9 mm) and clinopyroxene (up to 8 mm) phenocrysts are prominent, and apatite (≤300 μm) is common in more silicic flows and agglutinates (Table 2).

Waiaruhairiki Member (awh: between 152 and 150 ka). On the NE wall of the Mangahouhounui valley, a single 20-40 m thick section of Waiaruhairiki Member lavas crops out

between lower (~100 m) and upper (~150 m) successions of the Te Pakiraki Member (Figs. 3, 4) and the two members are inferred to have been erupted penecontemporaneously. This relationship is repeated in the headwall of the Mangahouhounui valley. Waiaruhairiki lavas also contain large plagioclase (up to 9 mm) and clinopyroxene (up to 8 mm) phenocrysts, which suggests similar magma assembly conditions, possibly in the same magma system as for earlier units, despite their distinct MgO concentrations (Tables 2, 3).

Tātaramoa Member (mtm: between 189 and 130 ka). A small exposure (<300 m of streambed) of basaltic-andesite lava in the Tahurangi Stream on NE Tongariro is the only known outcrop of the Tātaramoa Member (Fig. 4). Association with the Mangahouhounui Formation and its inferred age are based on petrography, with up to 9 mm-long plagioclase and clinopyroxene crystals. The geographic separation and mafic composition of this member relative to other Mangahouhounui Formation eruptives (Tables 2, 3) suggest that it was erupted from a flank vent, possibly Te Tatau peak, ~2 km uphill of the Tātaramoa Member outcrop (Fig. 2).

Undifferentiated Mangahouhounui Formation products (umh). Landscape-forming materials in the Mangahouhounui valley lower headwall are poorly exposed and have not been sampled because of burial by fan deposits and tephra. The stratigraphic levels of Te Pakiraki and Waiaruhairiki members in the Mangahouhounui valley headwall (Figs. 4) suggest that these undifferentiated materials are most likely to be part of the Mangahouhounui Formation (and are considered as such here), although they could alternatively be part of the older (290-189 ka) Haumata Formation (Figs. 3, 4).

3.2.5. Taiko Formation (between 133 and 52 ka) – TA

Products forming the Taiko Formation are lithologically diverse and spatially extensive, covering about 40% of Tongariro's edifice area (Fig. 8). They erupted from vent foci in the present-day Central Crater area; however, the dips (10-35 °) of Taiko Formation eruptives on Tongariro's upper edifice project back towards possible vent sources above 2000 m a.s.l., at least 100 m higher than any surviving landform in this area. This formation, therefore, represents the last phase of edifice growth for which the source vent(s) are not preserved whereas subsequent activity has been from vents presently visible in the landscape (Fig. 9). The missing edifice material is interpreted to have collapsed, forming at least part of the Te Whaiau Formation (section 3.2.7).

Rahuituki Member (arh: between 129 and 119 ka). This member is composed of andesite lavas on Tongariro's distal NE and NW flanks that extend up to 9 km from inferred source (Fig.

8). This distribution contrasts with older Mangahouhounui Formation eruptives that are generally confined to valley walls and have shorter runout distances (<6 km) or are buried.

Pungarara Member (apg: between 130 and 102 ka). The Pungarara Member comprises andesite lavas exposed on the upper SW Oturere valley wall (Fig. 8). The lavas contain traces of Fe-Ti oxide pseudomorphs after amphibole, which are absent in the Rahuituki Member.

Mangahouhouiti Member (mhi: between 130 and 96 ka). The Mangahouhouiti Member comprises basaltic-andesite lava flows and minor agglutinates that are only present on the planèze between the Mangahouhounui and Oturere valleys (Figs. 8, 9). Its limited distribution and mafic composition suggest that it probably erupted from a flank vent at the head of the planeze. It is distinguished by its high MgO content (~6.3 wt%: Tables 2, 3) and it is the most voluminous unit on Tongariro to contain olivine as the dominant phenocryst mineral. The Mangahouhouiti Member consists of two to three conformable lavas totalling 20-40 m thickness. It overlies the 195-189 ka Waipoa Member of the Haumata Formation (Fig. 9), consistent with the radiometric ages (Fig. 3).

Mangatepopo Member (amp: between 133 and 102 ka). The Mangatepopo Member consists of poorly exposed andesite lavas at ridgetop and valley-floor locations on Tongariro's upper edifice (Figs. 6, 8). Several disparate outcrops have been grouped together based mainly on their location and chemistry.

Te Porere Member (dtp: between 102 and 96 ka). This member consists of andesites and dacites that erupted from a vent area near present-day Central Crater onto N, E, SE, W and NW sectors of Tongariro (Figs. 8, 9). The Te Porere member represents part of central Tongariro that was grouped as a collection of undifferentiated materials and deposits by Townsend et al. (2017), but some of which were locally remapped by Cole et al. (2018). The Te Porere Member is lithologically diverse, being mostly lavas and agglutinates but with minor hyaloclastite, lapilli tuff and lapilli tuff breccia (Cole et al., 2018). The thickest sequence (100-120 m) is on the northern wall of the Mangatepopo valley where up to eight conformable lavas are inferred to overlie a 121 ± 12 ka Mangatepopo Member lava (Fig. 8). Here on the valley wall, Te Porere lavas display 'knuckles' where lava is locally overthickened by 5-10 m, which likely reflects ponding in void spaces at a lava-ice interface, as documented at neighbouring Ruapehu by Conway et al. (2015, 2016). In the upper SW Oturere valley Te Porere eruptives overlie 130-102 ka Pungarara Member andesites.

Otamangakau Member (aok: between 96 and 92 ka). The Otamangakau Member consists of andesite lavas and agglutinates, exposed primarily on Tongariro's NW flank and in the Mangahouhounui valley overlying the 102-96 ka Te Porere Member (Figs. 3, 8, 9). Otamangakau

Member andesites are compositionally similar to Te Porere Member eruptives but are distinguished by higher MgO concentrations (>3.1 wt%: Table 2).

Waitakatorua Member (awu: between 96 and 79 ka). The Waitakatorua Member principally forms a prominent ridge between the Oturere and Mangahouhounui valleys (Figs. 8, 9). It comprises lava flows intercalated with bedded lapilli tuffs (Fig. 7) collectively erupted from a vent focus near present-day Central Crater that alternated between subaerial and subaqueous (or subglacial) eruptive activity (Cole et al., 2018). North of the ridgeline, Waitakatorua lavas dip northwards into the Mangahouhounui valley at angles up to 35 ° (Fig. 9).

Te Rurunga Member (atr: between 92 and 84 ka). The Te Rurunga Member consists of andesitic welded agglutinates, scoria and lava. These overlie the 102-96 ka Te Porere and 96-92 ka Otamangakau members in a ~1 km^2 exposure on Tongariro's upper western slopes (Figs. 6, 8, 9).

Te Wakarikiariki Member (ati: between 86 and 79 ka). This member consists of isolated lavas on Tongariro's upper edifice and in the Mangahouhounui valley and is partly equivalent to Cole et al.'s (2018) dL unit (Figs. 8, 9). Some Te Wakarikiariki Member lavas are characterised by up to 7 mm plagioclase crystals, the sizes of which may suggest similar magma storage conditions to the older Mangahouhounui Formation (Table 2).

Rotopaunga Member (arp: between 79 and 61 ka). This member, synonymous with the Rotopaunga Formation of Townsend et al. (2017), includes lavas and agglutinates on Tongariro's NE, SE and W flanks (Figs. 6, 8, 9). It also includes hyaloclastites and lapilli tuff breccias on Tongariro's upper edifice mapped by Cole et al. (2018; their units ERh and ERltb) and attributed to a vent that alternated between subaerial and subglacial environments. Outcrops of the Rotopaunga Member triangulate to a source region in the present-day Central Crater area (Figs. 8, 9). All age results are consistent with field relations showing Rotopaunga Member eruptives overlying 102-96 ka Te Porere and 86-79 ka Te Wakarikiariki members (Fig. 3).

Te Tatau Member (att: between 61 and 52 ka). This member, synonymous with the Te Tatau Formation of Townsend et al. (2017), comprises andesitic scoria, agglutinates and lavas on Tongariro's upper NE flank (Fig. 8).

Undifferentiated Otukou lava (uol: between 91 and 79 ka). This comprises crystal-poor andesite lava exposed in a ~30 m section on the Waihi Fault scarp near Otukou settlement, ~9 km north of Tongariro (Fig. 8). Its composition is similar to the 86-79 ka Te Wakarikiariki and 61-52 ka Te Tatau members (see above), but field relations do not support their correlation because these members are separated by exposures of older lavas. Lecointre et al. (2002) suggested that the Otukou lava erupted from Maungakatote vent, ~15 km NNW of Tongariro, while other

possibilities include Rotopounamu and the Kakaramea edifice (Fig. 1). However, rock compositions (Cole, 1978; Cashman, 1979; Cole et al., 1983; this study) are sufficiently different to exclude correlating the Otukou lava with any of these vent foci in a manner compatible with field relations. The Otukou lava is overlain by the Te Whaiau Formation (Lecointre et al., 2002) but field relations with other eruptives have not been discovered.

3.2.7. Te Whaiau Formation (between 50 and 45 ka) – TW

The Te Whaiau Formation (Prebble, 1995; Lecointre et al., 2002; Townsend et al., 2017) is a widespread debris deposit on the NW Tongariro ring plain (Fig. 10; Table 4). A voluminous proportion of this material is inferred to be missing edifice material, probably from the Taiko Formation's vent area near Central Crater (Figs. 8, 9), although representative clast sampling is needed to assess which source materials comprise Te Whaiau Formation deposits. The formation contains metre-thick bedding in type locality outcrops on State Highway 47, ~8-9 km NW of Tongariro (Lecointre et al., 2002), indicating emplacement by multiple pulses. Because of poor exposure, the distribution of Te Whaiau Formation deposits, as mapped here (Fig. 10) and elsewhere (Lecointre et al., 2002; Townsend et al., 2017), may include unrelated ring plain deposits and fluvially reworked material.

3.2.8. Pukeonake Formation (between 40 and 30 ka) – PN

This formation (Pukeonake Formation of Townsend et al., 2017; Pukeonake lavas of Grindley, 1960) includes all eruptives from the vent now occupied by the Pukeonake scoria cone, beyond the western end of the Mangatepopo valley (Fig. 10). Other vents may exist, such as two ~20 m-high spatter mounds 800 m and 1100 m N of Pukeonake cone (Topping, 1974). Pukeonake eruptives are MgO-rich (7.9-8.9 wt%) basaltic-andesites with pyroxene-dominated phenocryst assemblages (Tables 2, 3) that include prominent forsteritic olivines (Hobden, 1997; Beier et al., 2017).

3.2.9. Mokomoko Formation (between 45 and 23 ka) – MM

This formation, as defined here, includes all products erupted from North Crater and Blue Lake that were previously mapped as separate formations (e.g. Gregg, 1960; Townsend et al., 2017). However, close similarities in eruptive ages (Table 1) and compositions (Tables 2, 3) lead us to group these eruptives into a single formation. Within this formation, member designations relate to vent locations: North Crater (Rangitaupahi and Mangatapate) and Blue Lake (Te Wai Whakaata).

Rangitaupahi Member (ari: between 45 and 36 ka). This member consists of andesite lavas, agglutinates and minor lapilli tuffs that form the North Crater landform, plus a 5 km-long lava flow to the NW of the cone (Figs. 6, 9, 10). Bedded lapilli tuffs and lavas exposed in the headwall of South Cirque, ~1 km SW of North Crater, are probably the member's oldest units. In contrast to the volumetrically dominant agglutinates and lavas elsewhere, these bedded lapilli tuffs are taken as evidence of initial subglacial eruptive activity from a proto-North Crater vent (Cole et al., 2018, 2019). During the later stages of North Crater activity that are related to the main cone formation, the eruptions deposited agglutinates up to 1 km from source during fire-fountaining and fed the lava to the NW. Lavas that fill the crater up to its overflow elevation are inferred to have once been part of a lava lake, now solidified (Townsend et al., 2017 and references therein). A 300 m diameter cap of Rangitaupahi Member material occurs on the ridge north of Blue Lake, ~1 km east of source, resting on Rotopaunga Member agglutinates (Figs. 3, 9).

Mangatapate Member (amt: between 36 and 24 ka). This member is represented by lava, agglutinates and proximal ejecta surrounding a 400 m-wide crater in the NW of the wider North Crater summit floor (Figs. 6, 9, 10). Holocrystalline lava, compositionally distinct from Rangitaupahi Member eruptives, is exposed on the crater's inner walls and was likely exposed during explosions that deposited the rim-draping agglutinates and surrounding blocks and ash.

Te Wai Whakaata Member (awv: between 33 and 23 ka). This member (synonymous with the Blue Lake Formation of Townsend et al., 2017) consists of andesite lavas and agglutinates erupted from a vent now occupied by Blue Lake, ~1 km east of North Crater (Figs. 9, 10). These eruptives are distinguished from other Mokomoko Formation products by their separate vent location. Like Rangitaupahi Member products, Te Wai Whakaata Member eruptives contain trace amounts of xenocrystic olivine and have major and trace element compositions that are indistinguishable within error of Mangatapate Member eruptives (Tables 2, 3). The Te Wai Whakaata Member includes a succession of conformable lavas that flowed eastwards from their vent into the Mangahouhounui valley. To the southeast, Te Wai Whakaata Member agglutinates overlie Waitakatorua Member lavas at an elevation 50-100 m above Blue Lake itself (~1740 m a.s.l.), which indicates deposition by fire-fountaining (Fig. 9). Te Wai Whakaata Member lavas on the floor of the Mangahouhounui valley appear to be overthickened by ≤20 m and are overlain by a thin (<20 m) veneer of till at ~1500 m a.s.l., suggesting possible interaction with the Mangahouhounui glacier at the time of eruption (e.g., Conway et al., 2015).

3.2.10. Te Maari Formation (before 25.4 ka to present) – TM

Synonymous with the Te Maari Formation of Townsend et al. (2017), this formation consists of three new members and an undifferentiated lava unit (Fig. 11). The members are defined by their stratigraphic positions with respect to regional tephra units: the 25.4 ka Oruanui Formation (Vandergoes et al., 2013), 17.5 ka Rerewhakaaitu Tephra (Lowe et al., 2013), c. 11 ka Pahoka-Mangamate sequence and 3.5 ka Papakai Tephra (Topping, 1974; Donoghue et al., 1995; Nairn et al., 1998) (Fig. 3). The age of the youngest member is constrained by dendrochronology and witnessed events (Topping, 1974; Scott and Potter, 2014).

Eruptives of the oldest three subunits (*undifferentiated Te Maari Formation products* [*utm*], *Paungaiti Member* [*api*] and *Heretoa Member* [*ahl*]) are andesites, whereas the younger *Mangatetipua Member* (*mgt*) is basaltic-andesite (summarised in Tables 2 and 3; details in Supplementary Materials). Unassigned pre-Oruanui (>25.4 ka) lava was possibly erupted from a now-buried vent located ~500 m east of Lower Te Maari Crater (Cronin, 1996; Townsend et al., 2017). This lava is overlain by the Paungaiti Member, erupted between 25.4 and 17.5 ka from the Lower Te Maari Crater (Cronin, 1996; Lecointre et al., 2004; Townsend et al., 2017) (Fig. 11). Paungaiti Member lava flowed ~6.5 km northwards, at least as far as Lake Rotoaira's current western shoreline (Townsend et al., 2017). Heretoa Member andesites then erupted between 11.0 and 3.5 ka from a vent ~500 m north of Lower Te Maari Crater, and flowed northwards, some at least as far as Lake Rotoaira's shoreline (Fig. 11). Subsequently, a basaltic-andesite lava was erupted from Upper Te Maari Crater at 1528 CE (Topping, 1974; Cole, 1978), preserved as a 3.5 km-long, leveed flow. This lava and all subsequent Te Maari eruptives, including products of the 2012 eruptions from Upper Te Maari Crater, collectively define the Mangatetipua Member (Fig. 11).

3.2.11. Makahikatoa Formation (~17.5 ka) – MK

The Makahikatoa Formation (following Townsend et al., 2017) consists of basaltic-andesite scoria, lava and spatter erupted from a vent on top of Pukekaikiore hill. The vent is located where the southern extension of the Waihi Fault crosses the Pukekaikiore landform (Figs. 1, 6). The age of Makahikatoa Formation is constrained by the rhyolitic 17.5 ka Rerewhakaaitu Tephra from Okataina (Lowe et al., 2013) that is interbedded between horizons of Makahikatoa Formation scoria (Topping, 1974). This age is consistent with field relations showing that Makahikatoa Formation lava diverted around Marine Isotope Stage (MIS) 2 moraines which were deposited prior to glacial retreat at ~18 ka (Eaves et al., 2016a).

3.2.12. Red Crater Formation (between 11.0 and 0.1 ka) – RC

This formation, synonymous with that of Townsend et al. (2017), comprises lava, spatter and scoria erupted from Red Crater at the head of the Oturere valley (Figs. 9, 11). Volcanic products on Tongariro's edifice record as many as 12 distinct eruptions (Topping, 1974; Shane et al., 2017) and nearby tephras suggest up to 16 eruptions since ~1660 CE (Moebis et al., 2011). Two new members are defined. The oldest is the *Te Ahititi Member* (*aht*), represented by valley-filling andesite lavas in the Oturere valley (Figs. 9, 11). The largest of these lavas (6.5 km long, volume of ~0.5 km^3: Stevens, 2002) yielded an $^{40}Ar/^{39}Ar$ age of 13 ± 12 ka (Table 1: TG088), consistent with the stratigraphy of overlying tephras (Topping, 1974). In contrast, post-232 CE eruptions produced basaltic-andesite scoria, spatter and lavas (Topping, 1974), mapped here as the *Te Rongo Member* (*mtr*), the lavas of which flowed only to 1.8 km from the vent in N, E and W directions (Figs. 9, 11).

3.2.13. Te Pupu Formation (between 7? ka and 1975 CE) – TP

Previously defined by Townsend et al. (2017), Te Pupu Formation comprises all edifice-forming products from the Ngauruhoe vent, including those forming the cone (Figs. 5, 6, 11). The formation is subdivided here into three members plus an undifferentiated unit, defined by two time markers: the 232 CE Taupō ignimbrite (Hogg et al., 2012) and European arrival in New Zealand (Fig. 3). The latter corresponds to the earliest "historical" lava eruption of Ngauruhoe in 1870 CE (Hobden et al., 2002). Te Pupu Formation comprises the *Papamānuka* (*mpa*: between 7? ka and 232 CE), *Toakakura* (*mtk*: between 232 CE and 1870 CE) and *Matariki* (*mmt*: from 1870 CE to 1975 CE) members. An *undifferentiated unit* (*utp*) encompasses all eruptives for which age relations are either undocumented or observations are unclear. Papamānuka Member lavas travelled the greatest distances, up to 5.5 km from the modern vent (Figs. 6, 11). These flows are demonstrably Holocene because they are present on the floors of valleys that were glaciated in MIS 2 (Eaves et al., 2016a) (Figs. 6, 11). Younger lavas flowed for shorter distances of <3 km (Toakakura Member) and <2 km (Matariki Member). All members are basaltic-andesites that have large degrees of compositional overlap (Tables 2, 3). Field mapping and compositional data were used by Hobden et al. (2002) to define five distinct groups of lavas. However, their study notes that older compositional "types" reappear after evidenced time-breaks, which precludes the assignment of ages from rock compositions alone. The equivalence between map units of this study and those of Hobden et al. (2002) and Townsend et al. (2017) is given in the Supplementary Materials.

4. Volumes of Tongariro eruptives

The areas, average thicknesses and volumes of edifice-forming units on Tongariro have been estimated for all mapped formations and members (Table 4). Volume estimation procedures are described fully in the Supplementary Materials. A total volume of 19 km^3 is calculated for all exposed mappable primary volcanic products, which does not include materials that are buried or missing. The volumes of three generations of moraines were also estimated assuming triangular cross-sectional profiles: these sum to ~0.8 km^3, or 4% of all mapped volcanic units. The Te Whaiau Formation, which is the most voluminous debris unit associated with Tongariro (Prebble, 1995; Lecointre et al., 2002; Townsend et al., 2017) has an estimated volume of ~0.6 km^3.

In comparison, the best estimate for Tongariro's total edifice volume is ~90 km^3, of which only 21% (i.e. 19 km^3) can be ascribed to mappable units. The total edifice value was computed as the difference between Tongariro's present-day shape and a base elevation datum that represents a horizon separating the volcanic edifice from older rocks. The elevation used is 750 m a.s.l, the midpoint between 900 and 600 m a.s.l. contours that define the base datum's northward-sloping surface from southern to northern Tongariro, respectively, as inferred from the elevations of flow fronts on distal lavas. This adopted value is consistent with gravity data that shows the volcanic base boundary at 750-850 m a.s.l. under Ngauruhoe (Robertson and Davey, 2018) and Tongariro (Miller and Williams-Jones, 2016), and gravity, aeromagnetic and magnetotelluric data (Cassidy et al., 2009) that indicate a horizon at 750-800 m a.s.l. that separates Tertiary sediments from overlying volcanic products in the saddle between Tongariro and Ruapehu.

The volume of ring plain deposits surrounding Tongariro is ~60 km^3, which corresponds to a ~550 km^2 toroidal area with Tongariro's edifice-forming materials omitted from the centre. The volume calculation here follows the same procedure as for the total edifice, with the same base datum value of 750 m a.s.l. Use of this value is justified because ring plain deposits are sourced from the volcano and because Tongariro sits in the centre of the rift zone (Fig. 1). Contributions of Ruapehu material to the Tongariro ring plain are unknown but expected to cancel out with Tongariro contributions to the Ruapehu ring plain. Greywacke sediments derived from rift walls are unlikely to have contributed significant volumes to the Tongariro ring plain because drainage systems prevent infilling of central rift areas. Instead, sediments produced from eroding rift walls are generally conveyed northwards away from Tongariro, as noted by their absence in central rift areas (Fig. 15; Townsend et al., 2017).

5. Discussion

5.1. Review of geochronological data

The twenty nine new $^{40}Ar/^{39}Ar$ age determinations on lava groundmass materials presented here (Table 1) build on thirty eight K/Ar age determinations by Hobden et al. (1996) and three by Stipp (1969), which were undertaken on whole-rock samples. Field relations and superposition provide an independent check on the accuracy of all radioisotopic age data from Tongariro (Supplementary Materials section S3), and at every locality where $^{40}Ar/^{39}Ar$ ages were determined on successively overlying units, ages are either within analytical error or the overlying units are younger.

Previous studies were unable to achieve the level of stratigraphic distinction developed here due to the low precision and variable accuracy of K/Ar age determinations compared with the $^{40}Ar/^{39}Ar$ dating method (e.g. Hobden, 1997; Townsend et al., 2017). Comparisons between K/Ar and $^{40}Ar/^{39}Ar$ ages reveal the factors leading to inaccuracies in the former, as shown for samples collected from the same stratigraphic units and analysed by both methods (Fig. 12a). For these comparisons, $^{40}Ar/^{39}Ar$ ages (weighted mean plateau ages [WMPA] or isochron ages) are considered appropriate (see the analysis of isochrons in the Supplementary Materials), and accurate because they are fully consistent with field relations where available. Total gas $^{40}Ar/^{39}Ar$ ages are usually close to preferred WMPA or isochron values, but not always (Table 1; Fig. 12b). Comparisons show that K/Ar ages are generally inaccurate for samples with low K_2O concentrations, particularly those with glass-bearing groundmass (Fig. 12b, c). K/Ar and $^{40}Ar/^{39}Ar$ age values systematically converge with increasing whole-rock K_2O concentrations, becoming consistently within error of each other for rocks with more than 1.8 wt% K_2O (Fig. 12b, c). Differences between $^{40}Ar/^{39}Ar$ and K/Ar ages do not systematically vary with the percentages of crystals in the K/Ar samples (Fig. 12d); the inaccuracies appear to be due to low K_2O concentrations and thus point at least in part to under-estimation of the reported error on those K/Ar experiments. Across all comparisons, whole-rock K/Ar age determinations on samples with holocrystalline groundmasses are consistently more accurate than glassy samples, for both low-K_2O and phenocryst-rich samples. This supports observations elsewhere that K/Ar and $^{40}Ar/^{39}Ar$ age determinations are most accurate for holocrystalline samples because of greater retention of Ar and K in crystalline materials (e.g. Hildreth and Lanphere, 1994; Gamble et al., 2003).

5.2. Evolution of the Tongariro edifice

5.2.1. Earliest eruptions

Tongariro's edifice has been constructed by lava flows and pyroclastic deposits since at least ~350 ka (Figs. 3, 4). The 512 ± 59 ka Otamatereinga Formation marks the earliest known eruptive activity expressed by materials exposed through the current edifice (Figs. 3, 4). However, the source of Otamatereinga Formation lavas is unclear and may or may not be coincident with present day Tongariro. Maungaku, Maungakatote, Kakaramea and Pihanga cones, NW to NE of Tongariro (Fig. 1), are precluded as sources due to elevation differences between these cones and the Otamatereinga Formation exposure. Geochemical data (Cole et al., 1983) for Pihanga, Kakaramea and Maungakatote edifices also have overlapping and non-unique chemistry that cannot be uniquely associated with Otamatereinga Formation compositions reported here. We infer that the Otamatereinga Formation represents an earlier independent centre that is now almost entirely buried by younger Tongariro eruptives.

Any eruptive activity that occurred before ~350 ka on Tongariro itself is not represented by any known materials exposed as part of the edifice. Undifferentiated materials in the Oturere and Mangahouhounui valleys, and on northern Tongariro, might represent old Tongariro eruptives but have not been sampled and are poorly exposed (Fig. 4). Drill cores from the Poutu-Tokaanu hydro canal, NE of Tongariro, penetrated andesite boulders in colluvium overlying a ~349 ka Whakamaru Group ignimbrite (Bayly and Quinlan, 1965; Brown et al., 1998; M. Rosenberg, pers. comm, 2018), consistent with a post-349 ka age (Downs et al., 2014) for Tongariro. However, available drill cores are not deep enough to examine pre-Whakamaru age volcanism in the southern TVZ.

The oldest materials that are confidently attributed to Tongariro are represented by the 349-293 ka Tupuna Formation. Although not found in-situ, petrographic features (abundant pseudomorphs after amphibole: Table 2) suggest that the hornblende-phyric Tupuna Formation is magmatically related to the 290-189 ka Haumata Formation and may represent the same magmatic system. The overlapping distributions of Haumata Formation eruptives and (buried) Tupuna Formation lavas on southern Tongariro (Fig. 4) imply that Tupuna Formation eruptives also originated from Tongariro. In addition, Tupuna Formation eruptives are compositionally similar to amphibole-phyric andesite boulders in the 349-309 ka Turakina Formation debris flow deposits exposed along the Whanganui coastline, 100 km SW of Tongariro (Gamble et al., 2003; Tost and Cronin, 2015). Tost et al. (2016) suggested that the Turakina Formation andesite boulders represented eruptives from Ruapehu because they have overlapping rare earth element (REE) abundances with Ruapehu's Te Herenga Formation (cf. Price et al., 2012), which Tost et al. (2016) show to be different from Tongariro eruptives in REE abundances. However, data from this study and Hobden (1997) show that Tupuna Formation (and Lower Tama Member of

the Haumata Formation) andesites have clear compositional overlap with both the Te Herenga (Price et al., 2012; Conway et al., 2018) and Turakina (Tost et al., 2016) formations (Fig. 13). On the basis of REE compositions alone, it is impossible to establish whether Turakina Formation boulders were sourced from Tongariro versus Ruapehu edifice materials (cf. Tost and Cronin, 2015; Tost et al., 2016).

Despite the inconclusive REE comparisons, a Tongariro source for the Turakina boulders is supported by two additional observations. First, amphibole and its pseudomorphs are absent in Ruapehu's Te Herenga Formation, whereas Turakina Formation andesite boulders contain abundant hornblende phenocrysts. In contrast, hornblende and its pseudomorphs are observed, respectively, in Tongariro's Tupuna and Haumata formations (Table 2), and therefore represent possible source materials of the Turakina Formation andesite clasts. Such mineralogies differ from Ruapehu Te Herenga Formation lavas which are characterised by clinopyroxene>plagioclase phenocryst assemblages (Hackett, 1985; Price et al., 2012; Conway et al., 2016). Second, the oldest $^{40}Ar/^{39}Ar$ age yet determined for Te Herenga Formation is 205 ± 27 ka (Gamble et al., 2003) whereas lava from Tupuna Formation yields an $^{40}Ar/^{39}Ar$ age of 304 ± 11 ka (Table 1). If the Turakina Formation andesite boulders represent material from Tongariro (e.g. Tupuna Formation), then volcanism at Tongariro must have initiated no later than 309 ka. Furthermore, in that scenario the proto-Turakina River catchment, which currently rises near Waiouru, ~20 km south of Ruapehu's summit, would have to have once been connected to Tongariro. This implies that Ruapehu has grown in the space between Tongariro and the current headwaters, largely since the time that the Turakina Formation debris flows were transported. Displacement on southern TVZ rift faults, such as the Rangipo, Shawcroft Road and Snowgrass faults (Villamor and Berryman, 2006), has probably also influenced drainage networks in this area.

5.2.2. 300-190 ka

From 290-190 ka, Haumata Formation lavas and pyroclastic materials erupted from a southern vent focus beneath modern Ngauruhoe (Figs. 3, 4, 5). However, the youngest part of the Haumata Formation (Waipoa Member) erupted from a vent further north, in the area of present-day Central Crater (Figs. 3, 4). Emplacement of the Waipoa Member between 195-189 ka was possibly contemporaneous with the emplacement of the Pukekaikiore Member between 200-190 ka from the southern vent focus. Both members probably tapped the same magma system because their compositions are indistinguishable within analytical uncertainty (Tables 2, 3).

The alternative hypothesis, that Waipoa Member lavas were erupted from a southern vent and travelled northwards over ice, is considered unlikely. Outcrops at equal elevation on both walls of the SE-trending Oturere valley only contain Waipoa Member lavas on the NE wall (Fig. 4). Given that that the dominant extensional faulting orientation is perpendicular to the Oturere valley (Fig. 1), Waipoa Member lavas should occur on the SW Oturere valley wall at similar elevations as the NE wall (up to 1560 m a.s.l.) if the vent location was near Ngauruhoe's present location, but this is not observed (Fig. 4). Outcrops of Waipoa Member lavas in the NE wall of the Oturere valley point back towards Central Crater and therefore this area is considered the most likely source vent location.

5.2.3. 190-130 ka

Eruptions continued from a vent focus in the area of present-day Central Crater between 189 and 130 ka with the emplacement of the Mangahouhounui Formation. Rock compositions ranging from basaltic-andesite to dacite characterise the 189-130 ka Te Pakiraki Member, while field relations and $^{40}Ar/^{39}Ar$ age determinations indicate that this member was emplaced in the Mangahouhounui valley contemporaneously with the 152-150 ka Waiaruhairiki Member. The occurrence of plagioclase and clinopyroxene phenocrysts up to 9 mm long in both members suggest a shared magmatic system and a discrete episode of high-MgO andesite production (5.4-6.2 wt%: Tables 2, 3). This episode was probably broadly contemporaneous with the emplacement of the Tātaramoa Member (basaltic-andesite) on NE Tongariro that was erupted from a flank vent, possibly at the Te Tatau summit on NE Tongariro (Fig. 2). The greater crystal concentrations, higher MgO and more silicic character of Waiaruhairiki Member andesites, relative to Tātaramoa Member basaltic-andesites, are consistent with a greater cargo of magnesian clinopyroxene crystals in Waiaruhairiki Member andesites (Table 2).

5.2.4. 130-50 ka

From 133-52 ka, eruptions represented by the Taiko Formation continued from the northern vent area, within the location of present-day Central Crater (Fig. 8). Missing edifice material relating to this eruptive period is inferred to be represented by debris in the Te Whaiau Formation (Fig. 10). Te Whaiau Formation debris flow deposits extend 10-15 km NW from the inferred vent area for the Taiko Formation and have independent age constraints indicating deposition between 50-45 ka, consistent with the minimum 52 ka age of the Taiko Formation (Fig. 3). The volume of the Te Whaiau Formation estimated here (~0.6 km^3: Table 4) is similar to the 0.5 km^3 estimated by Lecointre et al. (2002) who invoked a cone-shaped landform on

upper Tongariro that collapsed to explain the volume of volcaniclastic material in the debris flow deposits. An alternative to removal in the Te Whaiau Formation collapse is that erupted materials were emplaced onto a glacier in the Central Crater area and then conveyed away as debris. However, this interpretation requires additional vents encircling Central Crater to explain the distribution of Taiko Formation eruptives on all flanks (especially the voluminous 102-96 ka Te Porere Member). The lack of such vent-proximal landforms of Taiko Formation age in the surviving edifice counts against this alternative.

5.2.5. 50-14 ka

Subsequent edifice construction on Tongariro involved eruptions from vent areas that are still visible but were shorter-lived, more geographically dispersed and more numerous (Fig. 14). This interpretation should not be biased towards younger eruptives because pre-50 ka eruptives have excellent exposure, especially in the southern sector of the edifice where burial by post-50 ka eruptives is minimal (Figs. 4, 5, 6). Despite this, Tongariro's southern half shows no geologic evidence for numerous 300-50 ka vent areas (≤1 km^2) offset by distances >2 km in E-W or N-S directions, except for the Tātaramoa and Mangahouhouiti members that were possibly erupted from flank vents. In contrast, however, the 45-23 ka Mokomoko (North Crater and Blue Lake vents), >25.4 ka to 2012 CE Te Maari, ~17.5 ka Makahikatoa, 11-0.15 ka Red Crater and the 7(?) ka to 1975 CE Te Pupu (Ngauruhoe) formations were all erupted from distinct vents with inferred lifespans of <25 kyr (Fig. 14). Where these ages do not overlap, vent areas (≤1 km^2) are separated by >2 km, and therefore represent six vent areas since 50 ka relative to only two (or four) between 300 to 50 ka.

The previously inferred age range of North Crater between 25.4 and 14.0 ka is inconsistent with the findings of this study. Andesitic tephras of the Te Rato Lapilli (Topping, 1973) were correlated with proximal scoria deposits on North Crater and named Rt1, Rt2 and Rt3 by Shane et al. (2008). However, although these tephras occur between the 25.4 ka Oruanui and 14.0 ka Waiohau rhyolitic airfall deposits (ages from Vandergoes et al., 2013; Lowe et al., 2013), the age determination for the Mangatapate Member indicates that most of the North Crater cone was constructed prior to 30 ± 6 ka (Table 1). For both Rt1 and Rt2 to have erupted from North Crater, their ages must be between 25.4 ka (post-Oruanui) and 24 ka (minimum Mangatapate Member age at 2 s.d.: Table 1) which is considered unlikely. Similar arguments indicate that Blue Lake was also not a source vent for the Rt1-3 tephras, because of the 28 ± 5 ka age determination of the Te Wai Whakaata Member and its compositional similarity to North Crater eruptives (Rangitaupahi and Mangatapate members: Tables 1, 2). The vent

source(s) of Rt1-3 deposits therefore cannot be identified based on available published information.

5.2.6. Holocene activity

During the Holocene there have been at least three co-existing and contemporaneously active magma systems that are expressed as the Te Maari, Red Crater and Te Pupu (Ngauruhoe) formations (Figs. 3, 11), vented from three distinct areas separated by distances greater than 2 km. Other craters (predominantly phreatic or phreatomagmatic) also formed at Emerald Lakes (between Red Crater and Blue Lake: Fig. 2) and in South Cirque (e.g. Topping, 1974; Hobden, 1997; Nairn et al., 1998). Unit-specific studies of whole-rock compositions reveal several similarities (and differences) between these three formations (e.g. Hobden et al., 1999; Coote and Shane, 2016; Shane et al., 2017). The occurrence of multiple persistent vents erupting different magmas echoes similar findings at Ruapehu that show coexisting magmas of distinct compositions persisting throughout the volcano's lifespan (Gamble et al., 1999; Price et al., 2012; Conway et al., 2016). At Tongariro, however, there are general compositional similarities between the Te Maari, Red Crater and Te Pupu formations that have not been previously recognised. Early Holocene eruptives from Te Maari Craters (11-3.5 ka Heretoa Member) and Red Crater (11-1.8 ka Te Ahititi Member) are andesitic with a dominance of plagioclase phenocrysts over pyroxene over olivine (Table 2). Later Holocene eruptives in all three formations are basaltic-andesites that show increases in olivine proportions (Table 2). This is consistent with a volcano-wide input of mafic magma into dispersed magma reservoirs that, during crustal processing, acquired their own distinct compositions reflecting the idiosyncrasies of their specific reservoirs and residence times. Note that the Te Pupu Formation's maximum age is not well determined (cf. Moebis et al., 2011) and could be as young as 2.5 ka (Topping, 1974), which could explain the petrological distinctions between early and late Holocene eruptives mentioned above. If so, this would imply that the expression of volcanism at Tongariro has been significantly more dispersed spatially during the Holocene than earlier in the volcano's history, consistent with the waning longevities of vent systems over time (Fig. 14).

Similar suggestions of contemporaneous activity were inferred for the early Holocene Pahoka-Mangamate tephra sequence (Nairn et al., 1998). This sequence deposited from contemporaneous eruptions of magmas with diverse composition from separate vent foci between northern Tongariro and northern Ruapehu (>10 km linear vent alignment), which include Te Maari Crater(s), upper/central Tongariro vents, Tama lakes vents and Saddle Cone (Ruapehu) (Nakagawa et al., 1998). Bulk compositions of c. 11 ka Pahoka-Mangamate tephras

range from basaltic-andesite to dacite and the deposits contain <8 vol% crystals (Nakagawa et al., 1998), which contrasts with all edifice-forming materials in the Te Maari, Red Crater and Te Pupu formations that contain ≥20 vol% crystals (Table 2).

A further issue is the age of Ngauruhoe cone and its associated effusive and explosive eruptives. Originally interpreted to date from ~2.5 ka (Topping, 1974), it has since been proposed that Ngauruhoe's construction began at ~7 ka (Moebis et al., 2011). The older age boundary of ~7 ka was established by associating Ngauruhoe with tephra in the Papakai Formation that underlies the rhyolitic ~6.9 ka "Motutere Tephra" from Taupo (Moebis et al., 2011). This association was established from similarities in glass compositions between Ngauruhoe's 1954 CE and 1975 CE eruptions and the Papakai Formation material. These compositions contrast with those of glasses in the Tufa Trig Formation of Ruapehu (between 1.8 ka and 1314 CE: Donoghue et al., 1995; Donoghue and Neall, 1996; ages from Hogg et al., 2012 and Lowe et al., 2013) and Te Rongo Member scoria from Red Crater (between 1.8 ka and 1800 CE: Topping, 1973; Greve et al., 2016). However, in contrast to arguments by Moebis et al. (2011), available data indicates that Red Crater is a more likely source vent for the >6.9 ka Papakai Formation tephra. Whole-rock compositions from Red Crater's Te Ahititi Member (11-1.8 ka) are more evolved than the Ngauruhoe-sourced Papamānuka Member (>1.8 ka: *ahi* and *mpa* data in Table 3, above), which is the reverse situation to Red Crater versus Ngauruhoe tephra glass compositions reported by Moebis et al. (2011). In contrast, Moebis et al. (2011) excluded Red Crater as a possible source for >6.9 ka Papakai Formation tephra because its <1.8 ka compositions are more mafic than Ngauruhoe-sourced eruptives, but this argument is inapplicable for materials >1.8 ka. Isopach data for the Papakai Formation cannot distinguish between Ngauruhoe and Red Crater as source vents (Donoghue et al., 1995), and also indicate an additional contribution of Ruapehu-sourced material (Topping, 1973). Further tephra provenance and dating studies are needed to constrain the onset of Ngauruhoe cone-building.

5.3. Glacial history of Tongariro volcano

Tongariro has supported large ice masses during its lifespan, both within glacial and interglacial periods. Previous summit ice caps had thicknesses exceeding 150 m (Cole et al., 2018, 2019) and some valley-occupying glaciers were as thick as 250 m. Till was deposited during at least three periods of major glacial advance (Fig. 15) that are inferred to correlate with MIS 6 (191-130 ka), MIS 4 (71-57 ka) and MIS 3-2 (57-14 ka) (Lisiecki and Raymo, 2005; Eaves et al., 2016a). However, there is also field evidence for some ice coverage in the later part of MIS 7 (Townsend et al., 2017; this study) and MIS 5 (Townsend et al., 2017; Cole et al., 2018). Because

ice coverage determines the emplacement and preservation potential of erupted materials, syn-glacial edifice growth models can be used (in 'reverse') to infer past ice coverage (e.g. Lescinsky and Sisson, 1998; Conway et al., 2016). As shown in Fig. 16a, this framework is used here to infer paleoclimatic conditions on Tongariro, complemented by studies of moraine ages (Eaves et al., 2016a) and energy-balance ice coverage modelling results (Eaves et al., 2016b).

5.3.1 Penultimate glacial period

Haumata Formation eruptives (290-189 ka) are the oldest in-situ deposits attributed to a Tongariro vent source that display evidence for varied ice coverage when they were emplaced. Inferences regarding ice coverage on Tongariro before 220 ka are not accurate because volcanic materials older than this are poorly exposed (Fig. 4). Haumata Formation eruptives indicate persistent valley-filling glaciers in the Waihohonu and Mangatepopo valleys for at least the 220-190 ka period (later part of MIS 7: 243-191 ka, Lisiecki and Raymo, 2005). These glaciers appear to have thickened from ~60 to ~250 m over this 30 kyr period (Fig. 16a). From 220-214 ka, Tawhairauiki Member eruptives were probably emplaced next to ice because they overlie 229-220 ka Tutangatahiro Member eruptives, but do not fill any adjacent valleys. At this time, valley-filling glaciers were probably ~120 m thick. The 214-207 ka Upper Tama Member contains lavas that are ~60 m thick where they overlie Tawhairauiki Member lavas (Figs. 4, 5, but are locally overthickened to 200 m elsewhere, which implies that ice in the Tama lakes area was ~200 m thick during this period. Two ~100 m-thick lavas stacked between the Makahikatoa Stream and Mangatepopo valley, which correspond to the 207-200 ka Toatoa and 200-190 ka Pukekaikiore members (Figs. 4, 6), with rubbly upper surface and no apparent interior layering are taken to indicate lava impoundment by ice that must have been 200-250 m thick for the 207-190 ka period (Fig. 16a). These interpretations suggest growing ice coverage in the lead-up to the MIS 6 glacial period (Fig. 16b).

The transition from MIS 7 to MIS 6 (191 ka: Lisiecki and Raymo, 2005) closely coincides with the age boundary (189 ka) between the Haumata and Mangahouhounui formations (Fig. 16a, b). Eruptives of the 189-130 ka Mangahouhounui Formation are predominantly represented by ~250 m-thick successions of lavas, breccias and agglutinates on both sides of the Mangahouhounui valley (Fig. 4). In particular, the Te Pakiraki Member eruptives show some of the most conspicuous textures indicative of lava-ice interaction on Tongariro. In the Mangahouhounui valley, eruptive products are confined to the valley walls and display overthickened margins that occasionally bulge out towards the valley's centre. Locally, ridge-confined lavas contain horizontal columnar joints with ≤15-20 cm spacing (Fig. 7b), indicative of

ice-contact cooling (e.g. Lescinsky and Sisson, 1998; Conway et al., 2015). On both sides of the valley, the Te Pakiraki Member contains monomict volcaniclastic breccias with metre-scale layering, intercalated with coherent lavas (Fig. 7a) and plastering slopes parallel to the valley walls. These breccias are interpreted as being associated with the emplacement of lavas alongside glaciers. The presence of these breccias, and the absence of Mangahouhounui Formation eruptives in valley-floor positions and horizontal columnar-jointed lava, indicates ice thicknesses up to 250 m for the 189-130 ka period in the Mangahouhounui valley (Figs. 4, 7, 16a).

5.3.2. Complexities during the last interglacial and the lead-in to the last glacial period

Taiko Formation eruptives (133 to 52 ka) coincide with a complex part of New Zealand's Quaternary glacial history (Williams et al., 2015) and are broadly contemporaneous with the 130-57 ka MIS 5 period of Lisiecki and Raymo (2005) (Fig. 16a, b). Initial volcanism on Tongariro during this period is represented by the Rahuituki and Mangatepopo members (Table 1). The Mangatepopo Member lava (121 ± 12 ka) occurs in the floor of the Mangatepopo valley (Figs. 6, 8), which was repeatedly filled with ice during glacial periods (Eaves et al., 2016a) and the 129-119 ka Rahuituki Member lavas up to ~9 km outwards onto the NW and NE flanks. These observations suggest minimal ice coverage on Tongariro for the ~130-120 ka interval (Fig. 16a). In contrast, the Mangahouhouiti Member, dated at 117 ± 23 ka, and a younger lava from the Mangatepopo Member (109 ± 8 ka: Table 1) are confined to upper flank and planèze positions (Figs. 6, 8, 9), which would imply that valley ice thickened to 100-200 m between ~118-102 ka (Fig. 16a). These interpretations are consistent with the 128-118 ka Kaihinu Interglacial (MIS 5e), 117-109 ka stadial (MIS 5d) and the initially cool 108-98 ka interstadial (MIS 5c) periods defined by Williams et al. (2015) from speleothem records, following Barrell (2011).

The 102-96 ka Te Porere Member contains hyaloclastites and lapilli tuff breccias that are considered indicative of syn-glacial emplacement on upper edifice areas (e.g. Cole et al., 2018, 2019). Elsewhere, the Te Porere Member is comprised of lava flows confined to flanks and planèzes (Fig. 8). Tongariro's NW sector lacks surficially exposed moraines (Fig. 15), probably due to a later collapse of this part of the mountain and loss of any glacial record (sections 3.2.7, 5.2.4). Successions of Te Porere Member lavas in the Oturere and Mangatepopo valleys show evidence, such as being exposed on ridges and planèzes adjacent to the valley, but absent from the valley floor, for impoundment by ice that suggest glaciers up to ~120 m thick. Younger 96-79 ka Waitakatorua and 86-79 ka Te Wakarikiariki members were emplaced both subaerially and subglacially, as indicated by ice-impounded lavas and lapilli tuff breccias that are confined to

ridgetop positions (Waitakatorua Member – Fig. 7c; Te Wakarikiariki Member – 'dL' in Cole et al., 2018). Of these, the 96-79 ka Waitakatorua Member outcrops up to 240 m above the adjacent Oturere valley floor, suggesting an equivalent thickness of valley-filling ice (Fig. 16a). These age ranges correspond to the 97-88 ka stadial (MIS 5b) and 87-73 ka (MIS 5a) Otamangakau Interstadial periods, along with a possible glacial excursion between 84-80 ka (Williams et al., 2015), consistent with the inferred ice-dammed Te Wakarikiariki lava at 81 ± 5 ka (Cole et al., 2018; Table 1). The distribution and features of the 79-61 ka Rotopaunga Member indicate substantial ice-coverage on Tongariro for this period, with ice thicknesses in the upper Mangatepopo valley up to ~250 m (Fig. 16a). However, on Tongariro's upper edifice, alternating deposits of hyaloclastites, lapilli tuffs and coherent lavas in the 79-61 ka Rotopaunga Member indicate transitions between subglacial and subaerial eruptive activity, and therefore variable ice coverage during this period (Cole et al., 2018). A Rotopaunga Member lava erupted onto the NE flank, where no moraines have been discovered, was dated at 68 ± 15 ka (Table 1) and has no evidence for impoundment by ice. The mean value of this age result is close to the peak glacial advance (66-61 ka) within the New Zealand Last Glacial Cycle (72-62 ka) defined by Williams et al. (2015) (Fig. 16b). This indicates that either the $^{40}Ar/^{39}Ar$ age determination is inaccurate (with a true age closer to 80-70 ka), or that glaciers on the northern flank of Tongariro were minor during this period. On present data, the two possibilities cannot be decided between, but the latter is a distinct possibility because of no morainal evidence for MIS 4-2 glacial activity on this sector of the mountain either. In turn, however, the youngest Taiko Formation eruptives are represented by the 61-52 ka Te Tatau Member, which displays no evidence for syn-glacial emplacement, and coincides with the early part of the relatively warm Aurora Interstadial of Williams et al. (2015).

5.3.3. Last glacial period

Dip directions of eruptives within the Te Porere, Te Wakarikiariki, Waitakatorua and Rotopaunga members triangulate towards a summit vent position above 2000 m a.s.l. in the area of modern Central Crater. These eruptives are inferred to have formed a cone that collapsed to form the Te Whaiau Formation debris flows. Climate proxy records (Williams et al., 2015) suggest a warm period between 61-49 ka that probably caused a deglaciation event on Tongariro (late MIS 4/early MIS 3), as also inferred from the ice-free emplacement of Te Tatau Member eruptives. Earlier edifice growth prior to ~61 ka (see above) in the presence of ice may have created asymmetric and irregularly shaped landforms that were unstable (e.g. Townsend et al., 2017) once the ice was removed. Local examples of sector collapse deposits (e.g. the 10.5 ka

Murimoto and 5.2 ka Mangaio formations on Ruapehu: Palmer and Neall, 1989; Conway et al., 2016; Eaves et al., 2016a; Townsend et al., 2017) and globally (e.g. the Osceola Mudflow on Mount Rainier: Vallance and Scott; 1997) show that voluminous mass-wasting events commonly follow deglaciation events because the loss of supporting ice masses encourages the collapse of unstable landforms (Capra, 2006).

Edifice growth on upper Tongariro resumed with the 45-23 ka Mokomoko Formation. Lapilli tuff breccias and related masses of coherent lava (both in-situ and as proximal blocks) mapped as the 45-36 ka Rangitaupahi Member ('LTac', 'LTb', 'LTc', 'LTd' and 'LTo' in Cole et al., 2018) suggest that North Crater's initial eruptive activity was subglacial but later became subaerially emergent. Initially during this period, a summit ice thicknesses were >150 m (Fig. 16a; Cole et al., 2018). Despite this, MIS 4-2 moraines are not observed on NW Tongariro and may relate to a lack of suitable topography (i.e. pre-existing valleys) for accumulating glacial ice masses. It is also possible that North Crater was constructed soon after the collapse that produced the 50-45 ka Te Whaiau Formation at a time when remaining ice masses on the edifice were waning, as indicated by trends in inferred ice thicknesses (Fig. 16a). Such behaviour has been observed elsewhere when edifice collapse is quickly followed by rebuilding, such as Bezymianny (Girina, 2013) and Mount St. Helens (Swanson and Holcombe, 1990). Subsequent eruptive activity at Tongariro resumed with the 36-24 ka Mangatapate (North Crater vent) and 33-23 ka Te Wai Whakaata (Blue Lake vent) members which display limited evidence for syn-glacial emplacement. Te Wai Whakaata Member lavas in the Mangahouhounui valley have steep sides that imply minor overthickening and suggest that ice up to ~50 m thick was present in the valley floor (Figs. 9, 10, 16a). These lavas are capped by till in the upper Mangahouhounui valley (Fig. 15), which indicates some glacial advance after 28 ± 5 ka (Table 1).

The 45-23 ka period also coincides with the cosmogenic ^{3}He ages of moraines on Tongariro (Eaves et al., 2016a). The middle and the youngest moraines north of the Mangatepopo Valley (Figs. 6, 15) have mean ages between 57-45 ka (~MIS 3) and 30-18 ka (~MIS 2), respectively (Eaves et al., 2016a). During these periods, glaciers were up to ~120 m thick in the Mangatepopo and Oturere valleys as indicated by moraine elevations relative to valley floors (Figs. 15, 16a; Eaves et al., 2016a; Townsend et al., 2017). These periods of moraine deposition compare with South Island glacial advances at 49-47 ka and 32-28 ka as inferred by Williams et al. (2015), and are consistent with field observations for limited valley-confined ice masses when the 33-23 ka Te Wai Whakaata Member was erupted (Fig. 16a, b). The Tongariro glacial chronology is similar to Ruapehu for this period (Conway et al., 2016) where glaciers were ~80-120 m thick at equivalent elevations (~1400 to 1900 m a.s.l.). Glaciation at Tongariro

continued from ~28 to 18 ka as indicated by till draping 33-23 ka Te Wai Whakaata lavas (Mangahouhounui valley) and the presence of other Last Glacial moraines mapped around the lower parts of Tongariro (Fig. 15; Eaves et al., 2016a; Townsend et al., 2017). The products of subsequent activity show no evidence for interaction with ice.

Glacier modelling (Eaves et al., 2016b) indicates that average temperatures were 5 to 6 °C cooler than present during glacial advances at least for the ~57-45 ka and ~30-18 ka periods. The inferred presence of large 100-250 m valley-filling glaciers in Tongariro's history may have accumulated on a higher edifice, now down-dropped by rifting, or that at these times Ruapehu was a smaller edifice that imposed less of a rain-shadow effect for cold southerlies than at present (note that the dominant Holocene wind direction is to the NNE, as indicated by tephra isopachs: Nairn et al., 1998; Heinrich et al., 2020). During glacial periods, Tongariro had a summit ice cap and substantial valley-filling glaciers which influenced the distribution and textures of contemporaneous lavas and pyroclastic deposits.

5.4. Volume-time reconstructions and edifice growth

Volume-time patterns are widely used to examine variations in volcanic productivity (e.g. Singer et al., 1997, 2008; Maclennan et al., 2002; Sinton et al., 2005; Rawson et al., 2016; Yamamoto et al., 2018). However, in most studies there is little discussion of whether estimated volumes are truly representative of volcanic productivity (Frey et al., 2004; Vallance and Sisson, 2017; Calvert et al., 2018). For stratovolcanoes that have hosted glaciers, evidence for lava-ice interaction indicates that both the presence and absence of ice dictates where and how much erupted material is preserved (Lescinsky and Sisson, 1998; Hildreth and Fierstein, 2012; Conway et al., 2015). Whether or not volume-time trends reflect true variations in eruptive rates depends on whether the amount of preservation (or erosion) is consistent between periods of syn-glacial and inter-glacial edifice growth. To test this, time-volume trends at Tongariro are considered in the context of New Zealand's climate variability since ~230 ka (Fig. 16c).

Cumulative volume versus time patterns show five periods in Tongariro's history with contrasting edifice-building rates (Fig. 16c: source data in Table 4). Periods of higher and lower edifice-building rates alternate, corresponding to periods with relatively warm versus relatively cool climates. Shifts in edifice-building rates appear to closely coincide with the boundaries of marine isotope stages (Lisiecki and Raymo, 2005; Fig. 16b). Beginning at ~230 ka in late MIS 7 (interglacial), Tongariro's edifice-building rate was 0.08 km^3/kyr, which decreased to 0.02 km^3/kyr during MIS 6 (glacial). This accompanied inferred glacier thickening from ~100 m to ~250 m between ~220-190 ka (late MIS 7), and the persistence of 200-250 m-thick glaciers from

~190-130 ka (~MIS 6: section 5.3; Fig. 16a). An increase in edifice-building rate to 0.12 km^3/kyr occurs for the 130-70 ka period (MIS 5), during which glaciers expanded (up to ~250 m-thick) and contracted repeatedly, with an overall similar ice coverage compared to the ~190-130 ka interval (Fig. 16a). Between ~70-11 ka (MIS 4-2), the edifice-building rate decreased to 0.05 km^3/kyr, coincident with increased ice coverage (section 5.3). From ~11 ka to present the highest edifice-building rate (0.19 km^3/kyr) is observed for Tongariro during a period of no ice influence. These data show that higher edifice-building rates coincide with warmer climatic periods (and vice versa) and two contrasting interpretations are considered here.

(1) That higher edifice-building rates during warmer periods reflect true increases in eruptive rate that are triggered by reduced ice coverage on the volcano, linked to depressurisation of the magmatic system.
(2) The 'preservation bias'. When the volcano is covered in thick ice, the percentage of preserved erupted materials declines because materials emplaced onto ice will later be lost to the ring plain as debris (e.g. Hildreth and Fierstein, 2012; Conway et al., 2016) and not accounted for in edifice volume estimates.

For the first hypothesis, geochemical patterns should change in phase with changes in edifice-building rate and ice coverage. In Iceland, Maclennan et al. (2002) report contemporaneous increases in eruptive rates and increased variation in whole-rock MgO concentrations in early postglacial lavas (12-7 ka) versus glacial lavas (>12 ka). More recent lavas (<7 ka) revert to glacial-like eruptive rates and geochemistries, indicating that magmatic and volcanic responses (pulses) to deglaciation occur within ~5 kyr after significant reductions in ice coverage (maximum ice thicknesses up to 1 km in this example). Sinton et al. (2005) report similar geochemical and eruptive rate shifts between glacial (>12 ka), early postglacial (12-9 ka) and recent (<9 ka) lavas in the Western Volcanic Zone of Iceland. The behaviour of mid-latitude stratovolcanoes is unlikely to be as extreme, however, but if variations in MgO are synchronised with shifts in ice coverage this would support deglaciation as a trigger of increased eruptive rates during periods of warm climate.

At Tongariro, SiO_2 and MgO variations since ~230 ka (Fig. 16d, e) do not correlate with periods of warmer or cooler climate (Fig. 16b). Variations in MgO show periods of rapid increase followed by periods of slower decline (Fig. 16e), suggesting that increased mafic recharge events occur at Tongariro, but not at times of contemporary ice loss. Increases in MgO to maxima at ~230, ~160, ~88, ~56 ka and <12 ka occur within mid-MIS 7 (interglacial), mid-MIS 6 (glacial), mid-MIS 5 (interglacial), early MIS 4 (New Zealand's greatest Last Glacial advance: Williams et al., 2015) and the Holocene, respectively. Furthermore, high-MgO flank

vents appear around ~160 ka (189-130 ka), at ~117 ka, ~35 ka and ~17.5 ka, which are all periods of significant ice coverage on Tongariro (section 5.3). In contrast, SiO_2-time systematics do not show patterns over Tongariro's lifespan (Fig. 16d). Collectively, the data do not support the hypothesis that deglaciation acted as a trigger for increased eruptive rates on Tongariro and we infer that reduced edifice-building rates in ice-dominant periods reflect reduced completeness of the volcanic record. This inference contrasts with proposals that deglaciation triggers increased eruptive rates at mid-latitude stratovolcanoes (Singer et al., 1997, 2008; Rawson et al., 2016). It agrees, however, with other rigorous time-volume reconstructions that do not link deglaciation with increased effusive (Conway et al., 2016; Calvert et al., 2018) or explosive eruptive rates (Watt et al., 2013; Weller et al., 2015).

The ringplain volume adjacent to Tongariro, estimated here, is about 60 km^3, which can account for erupted but unpreserved material. If edifice building rates are on average 0.19 km^3/kyr, as for the Holocene period at Tongariro, missing volumes for the 230-0 ka interval are ~26 km^3; i.e. equivalent to Tongariro's total, visible in-situ edifice eruptive record. This estimate of erupted (but not in-situ) material, relative to ~60 km^3 of ringplain deposits, suggests that the ~34 km^3 of remaining ringplain deposits may reflect previously in-situ pyroclastic materials or materials older than 230 ka (or both).

The differences in edifice-building rates serve to quantify the preservation bias during ice-dominant periods. Ratios of edifice-building rates in ice-dominant versus warm climatic periods are 17 % (MIS 6/MIS 5) and 26 % (MIS 4-2/MIS 1) (Fig. 16b, c), reflecting the loss of material emplaced on to ice and subsequently conveyed to the ring plain. We suggest that comparable preservation rates may apply to other mid-latitude stratovolcanoes that have supported glaciers in their lifespans, contrasting with the view (e.g. Singer et al., 1997; Bablon et al., 2020) that erosion is the primary agent of volcanic record incompleteness at previously glaciated Quaternary mid-latitude stratovolcanoes. Moraine volumes on Tongariro (<1 km^3) equate to ≤5 % of the surficially exposed edifice-forming materials (Table 4) and <2 % of the total edifice (~90 km^3). Neighbouring Ruapehu has ~2 times more moraine (Townsend et al., 2017) associated with a ~150 km^3 total edifice (Gamble et al., 2003; Conway et al., 2016) so that till also accounts for <5 vol% of Ruapehu's volume. The overall stratovolcano growth model that holds for Tongariro is thus one whereby valley walls and other irregular or asymmetric landforms are primary landforms, constructed around existing ice masses: i.e., 'starfish'-shaped growth (Lescinsky and Sisson, 1998; Conway et al., 2015, 2016). This contrasts with traditional models that invoke periods of (perfect) cone-building alternating with periods of inactivity and glacial erosion (e.g. Hobden et al., 1996; Singer et al., 1997): i.e., episodic 'cone-building' growth.

The choice of growth model in any particular case study has fundamental implications for reconstructing erupted volumes.

5.5. Comparison of explosive versus effusive volcanism on Tongariro

Given that Holocene volcanic records for Tongariro are mostly complete, effusive and explosive volumes are compared here to assess how volcanic productivity is expressed for contrasting eruption styles. Eruptive activity since ~12 ka has produced ~6.2 km^3 of pyroclastic deposits, which would equate to ~3 km^3 dense-rock equivalent (DRE) (Topping, 1973; Donoghue et al., 1995; Nairn et al., 1998), plus ~1.5 km^3 of lava. Large explosive eruptions occurred in the early Holocene (12-11 ka Pahoka-Mangamate sequence: Nairn et al., 1998) with tephra volumes of ~5.9 km^3, about 4.5 km^3 (~2.3 km^3 DRE) of which came from Tongariro vents (Nairn et al., 1998). Other Tongariro-sourced regional deposits forming the Mangatawai, Ngauruhoe and Papakai tephra formations are ~1.3 km^3 bulk volume (Topping, 1973; Donoghue et al., 1995), while pyroclastic volumes in the Te Pupu, Red Crater and Te Maari formations are ~0.4 km^3. The second figure is based on areal proportions of effusive versus explosive material for these formations, as encountered during field investigations and inferred from aerial imagery for this study. Holocene effusive volumes (Te Pupu, Red Crater and Te Maari formations) are collectively ~1.6 km^3 (e.g. Table 4; these are effectively DRE volumes). Thus, explosive products are ~2 times more voluminous than effusive products for Tongariro during the Holocene. Tongariro's poorly examined and fragmentary pre-Holocene tephra record, however, precludes any meaningful consideration of effusive versus explosive volumes for Tongariro's longer-term history.

5.6. Ruapehu versus Tongariro growth history comparison

Tongariro and Ruapehu are located ~20 km apart along-axis in the TVZ arc and their growth histories are summarised in Table 5. In general, Tongariro is older, probably by ~100 kyr or more based on the data in this paper and Conway et al. (2016). Tongariro's edifice is more extensively faulted and consists of more dispersed vent locations than Ruapehu (Gómez-Vasconcelos et al., 2017; Townsend et al., 2017). Recent studies of Tongariro (this paper) and Ruapehu (Conway et al., 2016) show that eruptive activity at each volcano has been more or less continuous throughout their lifespans, in contrast to previous models of growth punctuated by periods of erosion at Tongariro (Hobden et al., 1996; Hobden, 1997) and eruptive hiatuses on Ruapehu (Hackett, 1985; Gamble et al., 2003).

The glacial histories of each volcano also differ (Table 5). Tongariro lacks moraines on its northern flank, which Ruapehu does have. Ruapehu also has a greater representation of younger moraines from MIS 2-1 (and has modern glaciers) whereas Tongariro has a greater representation of MIS 7-5 moraines (Eaves et al., 2016a; Conway et al., 2016; Townsend et al., 2017). Two possible explanations for these features are suggested. First, more productive edifice-building and MIS 4-1 glacial deposits may be obscuring MIS 6-5 moraines on Ruapehu. Second, when Ruapehu was a smaller edifice around ~200-150 ka (Conway et al., 2016; section 5.2.1), its rain-shadowing effect on Tongariro would have been weaker and Tongariro would have experienced comparatively greater snowfall.

Volume-time systematics cannot be compared in detail between each volcano because of contrasting assumptions and methods used for estimating volumes. However, Ruapehu has a larger edifice of ~150 km^3 constructed over ~200 kyr (Gamble et al., 2003; Conway et al., 2016) compared with ~90 km^3 for Tongariro that was constructed over ~300 kyr. These figures imply that Ruapehu's edifice-building rate has been about twice that of Tongariro's (Table 5). The eruptive volumes and proportions of explosive versus effusive eruptive outputs at each volcano contrast for the Holocene records (Table 5). Tongariro has erupted ~2 times more volume explosively (~3 km^3, DRE) than effusively (~1.6 km^3 DRE), whereas in contrast Ruapehu has erupted ~12 times more volume effusively (~9.6 km^3 DRE: Conway et al., 2016) than explosively (~1.5 km^3 bulk volume, ~0.8 km^3 DRE: Topping, 1973; Donoghue et al., 1995; Donoghue and Neall, 1996) in the Holocene. In terms of Holocene eruption rates, Ruapehu has been just over twice as productive as Tongariro, a ratio that appears to hold for the overall lifetime of each volcano.

6. Conclusions

Geological mapping, $^{40}Ar/^{39}Ar$ age determinations (Table 1) and whole-rock compositions from the Tongariro edifice and ring plain have been used to establish the composite stratovolcano's growth history. A new eruptive stratigraphy is presented (see Supplementary Materials for details), composed of twelve formations, thirty two constituent members and six undifferentiated units. Key findings are as follows.

(1) An inlier of basaltic-andesite on Tongariro's NW flank (Otamatereinga Formation: new), yielded a $^{40}Ar/^{39}Ar$ age determination of 512 ± 59 ka. This is the oldest dated in-situ material on the Tongariro edifice. However, the provenance of this lava is unclear and it may not have been erupted from Tongariro, instead representing an older, nearly buried centre.

(2) Hornblende-phyric andesite boulders of the Tupuna Formation (new), yield the oldest $^{40}Ar/^{39}Ar$ age determination for materials confidently attributed to Tongariro. Tupuna Formation andesites are correlated here with clasts in Turakina Formation debris flows (Tost and Cronin, 2015), which were deposited on the ring plain between 349-309 ka. Here, the source is inferred to be Tongariro rather than Ruapehu (cf. Tost and Cronin, 2015; Tost et al., 2016) as, at the time when the Turakina Formation debris flows were accumulating, Ruapehu probably did not exist, certainly not in its current form.

(3) New $^{40}Ar/^{39}Ar$ and previous K/Ar age determinations on in-situ lavas show that Tongariro's edifice-building eruptive history has been (more or less) continuous since ~230 ka, including during glacial periods.

(4) Comparisons between new $^{40}Ar/^{39}Ar$ and previous K/Ar age determinations show that holocrystalline lava samples yield results that are consistently more accurate than glassy samples. K/Ar age determinations become systematically more accurate with increasing K_2O concentrations, and are within error of $^{40}Ar/^{39}Ar$ determinations for rocks with >1.8 wt% K_2O, irrespective of whether the samples are glassy or holocrystalline. The abundance of phenocrysts (which can host melt inclusions with excess argon) does not correlate with the accuracy of whole-rock K/Ar age determinations.

(5) Tongariro has a total edifice volume of ~90 km^3, calculated above a base datum at ~750 m a.s.l. that separates volcanic materials from underlying sediments. The total ring plain volume surrounding the Tongariro edifice contains ~60 km^3 of material. The total volume of mapped units on Tongariro sums to 19 km^3, which is 21 % of the total edifice. The volume of moraines and glacial deposits is no more than 1 km^3.

(6) During periods of major ice coverage, edifice-building rates on Tongariro were only 17-26 % of edifice-building rates during warmer climatic periods. These shifts in edifice-building rates do not coincide with changes in erupted compositions, which supports that differences are due to a preservation bias and eruption style rather than effusion rates. It is inferred that materials erupted during periods of major ice coverage were emplaced onto ice masses and conveyed to the ring plain as debris, which accounts for reduced edifice-building rates during cool climatic periods. Edifice-building rates thus do not represent actual eruptive rates. Available data from Tongariro implies that deglaciations did not cause increases or decreases in eruptive rates.

(7) Rapid increases in whole-rock MgO concentrations to ~5-9 wt% are observed in Tongariro eruptives at ~230, ~160, ~117, ~88, ~56 ka and in the Holocene. This is in addition to the appearance of mafic flank vents at ~35 ka (Pukeonake Formation) and ~17.5 ka

(Makahikatoa Formation). These abrupt increases in MgO concentrations are followed by gradual declines in average erupted MgO concentrations and occur on irregular ~10-70 kyr cycles, which suggests that they result from episodes of enhanced mafic replenishment.

(8) Explosive output (~6.2 km^3 or 3 km^3 DRE) was ~2 times greater than effusive output (~2.0 km^3 or 1.6 km^3 DRE) during the Holocene at Tongariro. If the 12-11 ka Pahoka-Mangamate explosive eruptions are excluded, then Holocene effusive versus explosive output is about equal.

Declaration of competing interest

The authors declare that they have no conflict of interest.

CRediT authorship contribution statement

L.R. Pure: Conceptualization, Methodology, Formal analysis, Investigation, Resources, Data curation, Writing - original draft, Writing - review & editing. **D.B. Townsend**: Conceptualization, Methodology, Investigation, Supervision, Writing - review & editing. **G.S. Leonard**: Conceptualization, Methodology, Investigation, Supervision, Writing - review & editing. **C.J.N. Wilson**: Visualization, Project administration, Funding acquisition, Supervision, Writing - review & editing. **A.T. Calvert**: Methodology, Investigation, Writing - review & editing. **R.P. Cole**: Investigation, Writing - review & editing. **C.E. Conway**: Conceptualization, Writing - review & editing. **J.A. Gamble**: Conceptualization, Investigation, Supervision, Writing - review & editing. **T.'B'. Smith**: Supervision, Writing - review & editing.

Acknowledgements

LRP was supported by a PhD Scholarship from Victoria University of Wellington (VUW), with additional support from GNS Science and the ECLIPSE Programme funded by the New Zealand Ministry for Business, Innovation and Employment. Permission to undertake scientific sampling was granted by the Ngati Tūwharetoa iwi through the Department of Conservation to GNS Science. Analytical costs were supported by the Earthquake Commission of New Zealand grant 16/U735. We thank Andrew Galloway for assistance with field and lab work (pictured in Fig. 7a) and Drew Downs for help in the USGS dating facilities. LRP thanks the Antarctic Research Centre at VUW and the International Arctic Research Center at the University of Alaska, Fairbanks, for receipt of the S. T. Lee Travel Award. Anita Grunder, Jim Cole, Kevin Norton and four anonymous reviewers are thanked for their constructive comments which

improved this manuscript. Any use of trade, firm or product names is for descriptive purposes only and does not imply endorsement by the U.S. Government.

References

Bablon, M., Quidelleur, X., Samaniego, P., Pennec, J-L.L., Santamaría, S., Liorzou, C., Hidalgo, S., Eschbach, B. 2020. Volcanic history reconstruction in northern Ecuador: insights for eruptive and erosion rates on the whole Ecuadorian arc. Bull. Volcanol. 82, 11.

Barrell, D.J.A., 2011. Quaternary glaciers of New Zealand. In: Ehlers, J., Gibbard, P.L., Hughes, P.D. (Eds.), Developments in Quaternary Science, 15. Elsevier, Amsterdam, 1047–1064.

Bayly, T. F., Quinlan, L., 1965. Tokaanu – Poutu Canal j130. In: Tongariro Power Development Core Log, Ministry of Works and Development, Wellington, New Zealand, 8 pp.

Beavan, J., Wallace, L.M., Palmer, N., Denys, P., Ellis, S., Fournier, N., Hreinsdottir, S., Pearson, C., Denham, M., 2016. New Zealand GPS velocity field: 1995–2013. N.Z. J. Geol. Geophys. 59, 5-14.

Beier, C., Haase, K., Brandl, P.A., Krumm, S., 2017. Primitive andesites from the Taupo Volcanic Zone formed by magma mixing. Contrib. Mineral. Petrol. 172, 33.

Brown, S.J.A., Wilson, C.J.N., Cole, J.W., Wooden, J., 1998. The Whakamaru Group ignimbrites, Taupo Volcanic Zone, New Zealand: evidence for reverse tapping of a zoned silicic magmatic system. J. Volcanol. Geotherm. Res. 84, 1-37.

Calvert, A.T., Fierstein, J., Hildreth, W., 2018. Eruptive history of Middle Sister, Oregon Cascades, USA—product of a late Pleistocene eruptive episode. Geosphere 14, 2118-2139.

Capra, L., 2006. Abrupt climatic changes as triggering mechanisms of massive sector collapses. J. Volcanol. Geotherm. Res. 155, 329-333.

Cashman, K.V. (1979). Evolution of Kakaramea and Maungakatote volcanoes, Tongariro Volcanic Centre, New Zealand. Unpubl. MSc thesis, Victoria University of Wellington, Wellington, 152 pp.

Cassidy, J., Ingham, M., Locke, C.A., Bibby, H., 2009. Subsurface structure across the axis of the Tongariro Volcanic Centre, New Zealand. J. Volcanol. Geotherm. Res. 179, 233-240.

Cole, J.W., 1978. Andesites of the Tongariro Volcanic Centre, North Island, New Zealand. J. Volcanol. Geotherm. Res. 3, 121-153.

Cole, J. W. 1979. Chemical analyses of lavas and ignimbrites of the Taupo Volcanic Zone. Publ. Geol. Dept,, Victoria University of Wellington 13.

Cole, J.W., Cashman, K.V., Rankin, P.C., 1983. Rare-earth element geochemistry and the origin of andesites and basalts of the Taupo Volcanic Zone, New Zealand. Chem. Geol. 38, 255-274.

Cole, R.P., White, J.D.L., Conway, C.E., Leonard, G.S., Townsend, D.B., Pure, L.R., 2018. The glaciovolcanic evolution of an andesitic edifice, South Crater, Tongariro volcano, New Zealand. J. Volcanol. Geotherm. Res. 352, 55-77.

Cole, R.P., Ohneiser, C., White, J.D.L., Townsend, D.B., Leonard, G.S., 2019. Paleomagnetic evidence for cold emplacement of eruption-fed density current deposits beneath an ancient summit glacier, Tongariro volcano, New Zealand. Earth Planet. Sci. Lett. 522, 155-165.

Conway, C.E., 2016. Studies on the glaciovolcanic and magmatic history of Ruapehu volcano, New Zealand. Unpubl. PhD thesis, Victoria University of Wellington, Wellington, New Zealand. 207 pp.

Conway, C.E., Townsend, D.B., Leonard, G.S., Wilson, C.J.N., Calvert, A.T., Gamble, J.A., 2015. Lava-ice interaction on a large composite volcano: a case study from Ruapehu, New Zealand. Bull. Volcanol. 77, 21.

Conway, C.E., Leonard, G.S., Townsend, D.B., Calvert, A.T., Wilson, C.J.N., Gamble, J.A., Eaves, S.R., 2016. A high-resolution $^{40}Ar/^{39}Ar$ lava chronology and edifice construction history for Ruapehu volcano, New Zealand. J. Volcanol. Geotherm. Res. 327, 152-179.

Conway, C.E., Gamble, J.A., Wilson, C.J.N., Leonard, G.S., Townsend, D.B., Calvert, A.T., 2018. New petrological, geochemical, and geochronological perspectives on andesite-dacite magma genesis at Ruapehu volcano, New Zealand. Am. Mineral. 103, 565-581.

Coote, A.C., Shane, P., 2016. Crystal origins and magmatic system beneath Ngauruhoe volcano (New Zealand) revealed by plagioclase textures and compositions. Lithos 260, 107-119.

Cronin, S.J., 1996. Late Quaternary volcanic stratigraphy within a portion of the northeastern Tongariro Volcanic Centre. Unpubl. PhD thesis, Massey University, Palmerston North, New Zealand. 181 pp.

Davidson, J., de Silva, S., 2000. Composite volcanoes. In Sigurdsson, H. et al. (Eds), Encyclopedia of Volcanoes. Academic Press, San Diego, California, 663-681.

Donoghue, S.L., Neall, V.E., 1996. Tephrostratigraphic studies at Tongariro volcanic centre, New Zealand: an overview. Quat. Intl. 34, 13-20.

Donoghue, S.L., Neall, V.E., 2001. Late Quaternary constructional history of the southeastern Ruapehu ring plain, New Zealand. N.Z. J. Geol. Geophys. 44, 439-466.

Donoghue, S.L., Neall, V.E., Palmer, A.S., 1995. Stratigraphy and chronology of late Quaternary andesitic tephra deposits, Tongariro Volcanic Centre, New Zealand. J. Roy. Soc. N.Z. 25, 115-206.

Downs, D.T., Wilson, C.J.N., Cole, J.W., Rowland, J.V., Calvert, A.T., Leonard, G.S., Keall, J.M., 2014. Age and eruptive center of the Paeroa Subgroup ignimbrites (Whakamaru Group) within the Taupo Volcanic Zone of New Zealand. Geol. Soc. Am. Bull. 126, 1131-1144.

Dungan, M.A., Wulff, W., Thompson, R., 2001. Eruptive stratigraphy of the Tatara-San Pedro Complex, 36°S, Southern Volcanic Zone, Chilean Andes: reconstruction method and implications at long-lived arc volcanic centers. J. Petrol. 42, 555-626.

Eaves, S.R., Mackintosh, A.N., Winckler, G., Schaefer, J.M., Alloway, B.V., Townsend, D.B., 2016a. A cosmogenic ^{3}He chronology of late Quaternary glacier fluctuations in North Island, New Zealand (39°S). Quat. Sci. Rev. 132, 40-56.

Eaves, S.R., Anderson, B.M., Mackintosh, A.N., Doughty, A.M., Townsend, D.B., Conway, C.E., Winckler, G., Schaefer, J.M., Leonard, G.S., Calvert, A.T., 2016b. The Last Glacial Maximum in central North Island, New Zealand: paleoclimate inferences from 2D glacier modelling. Clim. Past 12, 943-960.

Edwards, B.R., Gudmundsson, M.T., Russell, J.K., 2015. Glaciovolcanism. In: Sigurdsson, H. et al. (Eds.), Encyclopedia of Volcanoes (2nd Ed.), Elsevier, Amsterdam, 377-393.

Fierstein, J., Hildreth, W., Calvert, A.T., 2011. Eruptive history of South Sister, Oregon Cascades. J. Volcanol. Geotherm. Res. 207, 145-179.

Frey, H.M., Lange, R.A., Hall, C.M., Delgado-Granados, H., 2004. Magma eruptions rates constrained by $^{40}Ar/^{39}Ar$ chronology and GIS for the Ceboruco-San Pedro volcanic field, western Mexico. Geol. Soc. Am. Bull. 116, 259-276.

Gamble, J.A., Wright, I.C., Baker, J.A., 1993. Seafloor geology and petrology in the oceanic to continental transition zone of the Kermadec-Havre-Taupo Volcanic Zone arc system, New Zealand. N.Z. J. Geol. Geophys. 36, 417-435.

Gamble, J.A., Wood, C.P., Price, R.C., Smith, I.E.M., Stewart, R.B., Waight, T., 1999. A fifty year perspective of magmatic evolution on Ruapehu Volcano, New Zealand: verification of open system behaviour in an arc volcano. Earth Planet. Sci. Lett. 170, 301-314.

Gamble, J.A., Price, R.C., Smith, I.E.M., McIntosh, W.C., Dunbar, N.W., 2003. $^{40}Ar/^{39}Ar$ geochronology of magmatic activity, magma flux and hazards at Ruapehu Volcano, Taupo Volcanic Zone, New Zealand. J. Volcanol. Geotherm. Res. 120, 271-287.

Gill, J., 1981. Orogenic Andesites and Plate Tectonics. Springer, New York, 390 pp.

Girina, O.A., 2013. Chronology of Bezymianny volcano activity, 1956-2010. J. Volcanol. Geotherm. Res. 263, 22-41.

Gómez-Vasconcelos, M.G., Villamor, P., Cronin, S.J., Procter, J., Kereszturi, G., Palmer, A., Townsend, D., Leonard, G., Berryman, K., Ashraf, S., 2016. Earthquake history at the eastern boundary of the south Taupo Volcanic Zone, New Zealand. N.Z. J. Geol. Geophys. 59, 522-543.

Gómez-Vasconcelos, M.G., Villamor, P., Cronin, S., Proctor, J., Palmer, A., Townsend, D., Leonard, G., 2017. Crustal extension in the Tongariro graben, New Zealand: insights into volcano-tectonic interactions and active deformation in a young continental rift. Geol. Soc. Am. Bull. 129, 1085-1099.

Gregg, D.R., 1960. The Geology of Tongariro Subdivision. New Zealand Geological Survey Bulletin 40.

Greve, A., Turner, G.M., Conway, C.E., Townsend, D.B., Gamble, J.A., Leonard, G.S., 2016. Palaeomagnetic refinement of the eruption ages of Holocene lava flows, and implications for the eruptive history of the Tongariro Volcanic Centre, New Zealand. Geophys. J. Int. 207, 702-718.

Grindley, G.W., 1960. Taupo [map]. Department of Scientific and Industrial Research. 1 map, scale 1:250,000. 1st ed. (Geological map of New Zealand 1:250,000; sheet 8).

Hackett, W.R., 1985. Geology and petrology of Ruapehu and related vents. Unpubl. PhD thesis, Victoria University of Wellington, Wellington, New Zealand. 312 pp.

Hackett, W.R., Houghton, B.F., 1989. A facies model for a Quaternary andesitic composite volcano: Ruapehu, New Zealand. Bull. Volcanol. 51, 51-68.

Heinrich, M., Cronin S.J., Pardo, N., 2020. Understanding multi-vent Plinian eruptions at Mt. Tongariro Volcanic Complex, New Zealand. Bull. Volcanol. 82, 30.

Hildreth, W., 1996. Kulshan caldera: a Quaternary subglacial caldera in the North Cascades, Washington. Geol. Soc. Am. Bull. 108, 786-793.

Hildreth, W., Fierstein, J., 2012. Eruptive history of Mount Katmai, Alaska. Geosphere 8, 1527-1567.

Hildreth, W., Lanphere, M.A., 1994. Potassium-argon geochronology of a basalt-andesite-dacite arc system: The Mount Adams volcanic field, Cascade Range of southern Washington. Geol. Soc. Am. Bull. 106, 1413-1429.

Hitchcock, D.W., Cole, J.W., 2007. Potential impacts of a widespread subplinian andesitic eruption from Tongariro volcano, based on a study of the Poutu Lapilli. N.Z. J. Geol. Geophys. 50, 53-66.

Hobden, B. J., 1997. Modelling magmatic trends in space and time: eruptive and magmatic history of the Tongariro volcanic complex. Unpubl. PhD thesis, University of Canterbury, Christchurch, New Zealand. 508 pp.

Hobden, B.J., Houghton, B.F., Lanphere, M.A., Nairn, I.A., 1996. Growth of the Tongariro volcanic complex: new evidence from K-Ar age determinations. N.Z. J. Geol. Geophys. 39, 151-154.

Hobden, B.J., Houghton, B.F., Davidson, J.P., Weaver, S.D., 1999. Small and short-lived magma batches at composite volcanoes: time windows at Tongariro volcano, New Zealand. J. Geol. Soc. London, 156, 865-868.

Hobden, B.J., Houghton, B.F., Nairn, I.A., 2002. Growth of a young, frequently active composite cone: Ngauruhoe volcano, New Zealand. Bull. Volcanol. 64, 392-409.

Hogg, A., Lowe, D., Palmer, J., Boswijk, G., Ramsey, C.B., 2012. Revised calendar date for the Taupo eruption derived by ^{14}C wiggle-matching using a New Zealand ^{14}C calibration data set. Holocene 22, 439-449.

Jiao, R., Seward, D., Little, T.A., Kohn, B.P., 2014. Thermal history and exhumation of basement rocks from Mesozoic to Cenozoic subduction cycles, central North Island, New Zealand. Tectonics 33, 1920-1935.

Jicha, B.R., Coombs, M.L., Calvert, A.T., Singer, B.S., 2012. Geology and $^{40}Ar/^{39}Ar$ geochronology of the medium- to high-K Tanaga volcanic cluster, western Aleutians. Geol. Soc. Am. Bull. 124, 842-856.

Lecointre, J.A., Neall, V.E., Wallace, R.C., Prebble, W.M., 2002. The 55- to 60-ka Te Whaiau Formation: a catastrophic, avalanche-induced, cohesive debris-flow deposit from proto-Tongariro volcano, New Zealand. Bull. Volcanol. 63, 509-525.

Lecointre, J.A., Neall, V.E., Wallace, R.C., Elliot, M.B., Sparks, R., 2004. Late Quaternary evolution of the Rotoaira Basin, northern Tongariro ring plain, New Zealand. N.Z. J. Geol. Geophys. 47, 549-565.

Lee, J.M., Bland, K J., Townsend, D.B., and Kamp, P.J.J., 2011. Geology of the Hawkes Bay area [map]. Lower Hutt (NZ), Institute of Geological and Nuclear Sciences. 1 sheet + 93 pp., scale 1:250,000. (Institute of Geological & Nuclear Sciences 1:250,000 map 8).

Lescinsky, D.T., Sisson, T.W., 1998. Ridge-forming, ice-bounded lava flows at Mount Rainier, Washington. Geology 26, 351-354.

Lisiecki, L.E., Raymo, M. E., 2005. A Pliocene-Pleistocene stack of 57 globally distributed benthic $\delta^{18}O$ records. Paleoceanography 20, PA1003.

Lowe, D.J., Blaauw, M., Hogg, A.G., Newnham, R.M., 2013. Ages of 24 widespread tephras erupted since 30,000 years ago in New Zealand, with re-evaluation of the timing and palaeoclimatic implications of the Lateglacial cool episode recorded at Kaipo bog. Quat. Sci. Rev. 74, 170-194.

Maclennan, J., Jull, M., McKenzie, D., Slater, L., Grönvold, K., 2002. The link between volcanism and deglaciation in Iceland. Geochem. Geophys. Geosyst. 3, 1062-1087.

Mathews, W.H., 1952. Ice-damned lavas from Clinker Mountain, southwestern British Columbia. Am. J. Sci. 250, 553-565.

McArthur, J.L., Shepherd, M.J., 1990. Late Quaternary glaciation of Mt. Ruapehu, North Island, New Zealand. J. Roy. Soc. N.Z. 20, 287-296.

McDonough, W.F., Sun, S.-s. (1995). The composition of the Earth. Chem. Geol. 120, 223-253.

Miller, C.A., Williams-Jones, G., 2016. Internal structure and volcanic hazard potential of Mt. Tongariro, New Zealand, from 3D gravity and magnetic models. J. Volcanol. Geotherm. Res. 319, 12-28.

Moebis, A., Cronin, S.J., Neall, V.E., Smith, I.E.M., 2011. Unravelling a complex volcanic history from fine-grained, intricate Holocene ash sequences at the Tongariro Volcanic Centre, New Zealand. Quat. Int. 246, 352-363.

Nairn, I.A., Kobayashi, T., Nakagawa, M., 1998. The ~10 ka multiple vent pyroclastic eruption sequence at Tongariro Volcanic Centre, Taupo Volcanic Zone, New Zealand: Part 1. Eruptive processes during regional extension. J. Volcanol. Geotherm. Res. 86, 19-44.

Nakagawa, M., Nairn, I.A., Kobayashi, T., 1998. The ~10 ka multiple vent pyroclastic eruption sequence at Tongariro Volcanic Centre, Taupo Volcanic Zone, New Zealand: Part 2. Petrological insights into magma storage and transport during regional extension. J. Volcanol. Geotherm. Res. 86, 45-65.

Nicol, A., Mazengarb, C., Chanier, F., Rait, G., Uruski, C., Wallace, L., 2007. Tectonic evolution of the active Hikurangi subduction margin, New Zealand, since the Oligocene. Tectonics 26, 1-24.

Palmer, B.A., Neall. V.E., 1989. The Murimotu Formation–9500 year old deposits of a debris avalanche and associated lahars, Mount Ruapehu, North Island, New Zealand. N.Z. J. Geol. Geophys. 32, 477-486.

Patterson, D.B., Graham, I.J., 1988. Petrogenesis of andesitic lavas from Mangatepopo valley and Upper Tama Lake, Tongariro volcanic centre, New Zealand. J. Volcanol. Geotherm. Res. 35, 17-29.

Pillans, B., 1983 . Upper Quaternary marine terrace chronology and deformation, South Taranaki, New Zealand. Geology 11, 292-297.

Prebble, W.M., 1995. Landslides in New Zealand. In: Bell, D.H. (Ed.), Landslides: Proc. 6th Intl. Symp., Feb 10-14 1992, Christchurch, New Zealand, vol. 3, 2101-2123.

Price, R.C., Gamble, J.A., Smith, I.E.M., Maas, R., Waight, T., Stewart, R.B., Woodhead, J., 2012. The anatomy of an andesite volcano: a time–stratigraphic study of andesite petrogenesis and crustal evolution at Ruapehu volcano, New Zealand. J. Petrol. 53, 2139-2189.

Pure, L.R., 2020. The volcanic and magmatic evolution of Tongariro volcano, New Zealand. Unpubl. PhD thesis, Victoria University of Wellington, Wellington, New Zealand, 436 pp.

Rawson, H., Pyle, D.M., Mather, T.A., Smith, V.S., Fontijn, K., Lachowycz, S.M., Naranjo, J.A., 2016. The magmatic and eruptive response of arc volcanoes to deglaciation: insights from southern Chile. Geology 44, 251-254.

Robertson, E.I., Davey, F.J., 2018. The basement morphology under Tongariro National Park, southern Taupo Volcanic Zone. N.Z. J. Geol. Geophys. 61, 570-577.

Scott, B.J., Potter, S.H., 2014. Aspects of historical eruptive activity and volcanic unrest at Mt. Tongariro, New Zealand: 1846-2013. J. Volcanol. Geotherm. Res. 286, 263-276.

Shane, P., Doyle, L.R., Nairn, I.A., 2008. Heterogeneous andesite-dacite ejecta in 26-16.6 ka pyroclastic deposits of Tongariro volcano, New Zealand: the product of multiple magma-mixing events. Bull. Volcanol. 70, 517-536.

Shane, P., Maas, R., Lindsay, J., 2017. History of Red Crater volcano, Tongariro Volcanic Centre (New Zealand): abrupt shift in magmatism following recharge and contrasting evolution between neighbouring volcanoes. J. Volcanol. Geotherm. Res. 340, 1-15.

Singer, B.S., Thompson, R.A., Dungan, M.A., Feeley, T.C., Nelson, S.T., Pickens, J.C., Brown, L.L., Wulff, A.A., Davidson, J.P., Metzger, J., 1997. Volcanism and erosion during the past 930 ky at the Tatara–San Pedro complex, Chilean Andes. Geol. Soc. Am. Bull. 109, 127-142.

Singer, B.S., Jicha, B.R., Harper, M.A., Naranjo, J.A., Lara, L.E., Moreano-Roa, H., 2008. Eruptive history, geochronology, and magmatic evolution of the Puyehue-Cordón-Caulle volcanic complex, Chile. Geol. Soc. Am. Bull. 120, 599-618.

Sinton, J., Grönvold, K., Sæmundsson, K., 2005. Postglacial eruptive history of the Western Volcanic Zone, Iceland. Geochem. Geophys. Geosyst. 6, Q12009.

Sisson, T.W., Salters, V.J.M., Larson, P.B., 2014. Petrogenesis of Mount Rainier andesite: magma flux and geologic controls on the contrasting differentiation styles at stratovolcanoes of the southern Washington Cascades. Geol. Soc. Am. Bull. 126, 122-144.

Stevens, N.F., 2002. Emplacement of the large andesite lava flow in the Oturere Stream valley, Tongariro Volcano, from airborne interferometric radar. N.Z. J. Geol. Geophys. 45, 387-394.

Stipp, J.J., 1969. The geochronology and petrogenesis of the Cenozoic volcanics of the North Island, New Zealand. Unpubl. PhD thesis, Australian National University, Canberra, Australia. 438 pp.

Swanson, D.A., Holcomb, R.T., 1990. Regularities in growth of the Mount St. Helens dacite dome, 1980–1986. In: Fink, J.H. (Ed.), Lava Flows and Domes, IAVCEI Proc. Volcanol. 2, 3-24.

Topping, W.W., 1973. Tephrostratigraphy and chronology of late Quaternary eruptives from the Tongariro Volcanic Centre, New Zealand. N.Z. J. Geol. Geophys. 16, 397-423.

Topping, W.W., 1974. Some aspects of Quaternary history of Tongariro Volcanic Centre. Unpubl. Ph.D. thesis, Victoria University of Wellington, Wellington, New Zealand, 245 pp.

Tost, M., Cronin, S.J., 2015. Linking distal volcaniclastic sedimentation and stratigraphy with the development of Ruapehu volcano, New Zealand. Bull. Volcanol. 77, 94.

Tost, M., Price, R.C., Cronin, S.J., Smith, I.E.M., 2016. New insights into the evolution of the magmatic system of a composite andesite volcano revealed by clasts from distal mass-flow deposits: Ruapehu volcano, New Zealand. Bull. Volcanol. 78, 38.

Townsend, D.B., Leonard, G.S., Conway, C.E., Eaves, S.R., Wilson, C.J.N., 2017. Geology of the Tongariro National Park area. Lower Hutt (NZ): GNS Science. 1 sheet + 109 pp., scale 1:60,000. (GNS Science geological map 4).

Vallance, J.W., Scott, K.M., 1997. The Osceola Mudflow from Mount Rainier: Sedimentology and hazard implications of a huge clay-rich debris flow. Geol. Soc. Am. Bull. 109, 143-163.

Vallance, J.W., Sisson, T.W., 2017. Geologic Field-Trip Guide to Volcanism and its Interaction with Snow and Ice at Mount Rainier, Washington. Draft report for IAVCEI General Assembly, Portland, Oregon, 14-18 August 2017. U.S. Department of the Interior and U.S. Geological Survey, 101 pp.

Vandergoes, M.J., Hogg, A.G., Lowe, D.J., Newnham, R.M., Denton, G.H., Southon, J., Barrell, D.J.A., Wilson, C.J.N., McGlone, M.S., Allan, A.S.R., Almond, P.C., Petchey, F., Dabell,

K., Dieffenbacher-Krall, A.C., Blaauw, M., 2013. A revised age for the Kawakawa/Oruanui tephra, a key marker for the Last Glacial Maximum in New Zealand. Quat. Sci. Rev. 74, 195-201.

Villamor, P., Berryman, K., 2006. Evolution of the southern termination of the Taupo Rift, New Zealand. N.Z. J. Geol. Geophys. 49, 23-37.

Villamor, P., Berryman, K.R., Ellis, S.M., Schreurs, G., Wallace, L.M., Leonard, G.S., Langridge, R.M., Ries, W.F., 2017. Rapid evolution of subduction-related continental intra-arc rifts: the Taupo rift, New Zealand. Tectonics 36, 2250-2272.

Wahyudin, D., 1993. Volcanology and petrology of the Tama Lakes area, Tongariro Volcanic Centre, New Zealand. Unpubl. MSc thesis, Victoria University of Wellington, Wellington, New Zealand, 153 pp.

Wallace, L.M., Beavan, J., McCaffrey, R., Darby, D.J., 2004. Subduction zone coupling and tectonic block rotations in the North Island, New Zealand. J. Geophys. Res. 109, B12406.

Watt, S.F.L., Pyle, D.M., Mather, T.A., 2013. The volcanic response to deglaciation: Evidence from glaciated arcs and a reassessment of global eruption records. Earth-Sci. Rev. 122, 77-102.

Weller, D.J., Miranda, C.G., Moreno, P.L., Villa-Martínez, R., Stern, C.R., 2015. Tephrochronology of the southernmost Andean Southern Volcanic Zone, Chile. Bull. Volcanol. 77, 107.

Williams, P.W., McGlone, M., Neil, H., Zhao, J.-X., 2015. A review of New Zealand palaeoclimate from the Last Interglacial to the global Last Glacial Maximum. Quat. Sci. Rev. 110, 92-106.

Wilson, C J.N., Houghton, B.F., McWilliams, M.O., Lanphere, M.A., Weaver, S.D., Briggs, R.M., 1995. Volcanic and structural evolution of Taupo Volcanic Zone, New Zealand: a review. J. Volcanol. Geotherm. Res. 68, 1-28.

Yamamoto, T., Kudo, T., Isizuka, O., 2018. Temporal variations in volumetric magma eruption rates of Quaternary volcanoes in Japan. Earth Planets Space 70, 65.

Table 1. Summary of new $^{40}Ar/^{39}Ar$ age determinations for Tongariro lavas.

Sample	Formation – Member (member abbreviation)[1]	Plateau age[2]				Isochron age[2]				Total gas age
		n/N	$\%^{39}Ar$	MSWD	(ka ± 2 s.d.)	$\%^{39}Ar$	MSWD	(ka ± 2 s.d.)	$^{40}Ar/^{36}Ar_i$ (± 2 s.d.)	(ka ± 2 s.d.)
TG088	RC – Te Ahititi (**ahi**)	6/10	77.8	2.07	**12.9 ± 11.8**	77.8	2.40	8.3 ± 25.4	301.4 ± 22.4	21.8 ± 10.2
LP147	MM – Te Wai Whakaata (**aww**)	11/11	100.0	0.46	**28.3 ± 5.2**	100.0	0.50	29.3 ± 7.6	298.0 ± 3.5	27.2 ± 6.0
LP151	MM – Mangatapate (**amt**)	5/10	69.3	0.41	**30.1 ± 6.0**	69.3	0.49	26.8 ± 14.8	305.0 ± 33.7	51.6 ± 6.2
GL2223	TA – Te Tatau (**att**)	11/11	100.0	1.31	**56.2 ± 4.6**	100.0	1.05	59.5 ± 5.4	296.3 ± 2.8	54.8 ± 4.8
LP211	TA – Rotopaunga (**arp**)	9/10	98.9	3.47	86.4 ± 12.4	**98.9**	**1.60**	**68.3 ± 15.4**	319.3 ± 18.4	96.0 ± 7.6
GL2007	TA – Rotopaunga (**arp**)	9/10	97.4	0.44	**76.1 ± 3.5**	97.4	0.38	78.4 ± 5.9	291.2 ± 10.1	73.3 ± 4.1
RPC110	TA – Te Wakarikiariki (**ati**)	4/11	63.6	0.98	**80.6 ± 4.8**	63.6	1.13	74.8 ± 15.2	304.0 ± 15.7	82.9 ± 6.0
LP062	undifferentiated Otukou lava (**uol**)	10/10	100.0	0.87	**85.0 ± 6.0**	100.0	0.86	89.7 ± 11.6	296.7 ± 4.4	83.8 ± 6.6
LP023	TA – Te Rurunga (**atr**)	6/11	58.7	1.07	**87.5 ± 4.2**	58.7	0.79	84.2 ± 6.2	304.0 ± 9.0	96.0 ± 4.0
LP103	TA – Te Porere (**dtp**)	4/10	71.2	0.69	**98.9 ± 2.6**	71.2	0.96	101.1 ± 14.2	290.7 ± 55.7	98.5 ± 3.0
LP010	TA – Mangatepopo (**amp**)	8/10	96.4	1.80	**108.5 ± 8.4**	96.4	1.73	102.9 ± 15.6	305.1 ± 21.2	119.1 ± 7.2
MSR15019	TA – Mangahouhouiti (**mhi**)	10/11	99.2	0.89	**116.8 ± 23.4**	99.2	0.88	141.4 ± 56.2	297.3 ± 3.1	108.0 ± 25.4
LP250	TA – Mangatepopo (**amp**)	7/10	70.5	2.12	**121.1 ± 12.2**	70.5	1.83	114.3 ± 14.6	307.0 ± 21.4	169.2 ± 9.0
LP214	TA – Rahuituki (**arh**)	7/10	75.9	0.77	**124.4 ± 4.8**	75.9	0.78	124.2 ± 5.4	297.4 ± 6.2	135.0 ± 5.6
TG084	MH – Te Pakiraki (**dpk**)	8/10	90.5	0.84	**136.5 ± 7.0**	90.5	0.79	130.8 ± 11.8	304.2 ± 12.6	153.3 ± 7.6
LP245	MH – Waiaruhairiki (**awh**)	7/10	81.8	0.30	**147.3 ± 7.4**	81.8	0.35	148.9 ± 17.4	296.9 ± 17.2	174.9 ± 7.6
LP234	MH – Te Pakiraki (**dpk**)	8/10	96.0	0.92	**151.8 ± 4.0**	96.0	0.62	146.7 ± 7.4	310.5 ± 18.0	158.9 ± 4.6
LP118	MH – Te Pakiraki (**dpk**)	8/10	88.2	1.35	**155.4 ± 5.2**	88.2	1.48	157.1 ± 13.4	297.0 ± 11.3	152.6 ± 5.0
LP129	MH – Te Pakiraki (**dpk**)	10/10	100.0	1.13	**164.9 ± 5.8**	100.0	1.23	166.2 ± 12.2	296.8 ± 11.5	164.9 ± 5.8
LP239	MH – Te Pakiraki (**dpk**)	3/10	58.2	2.43	203.8 ± 9.6	**58.2**	**1.12**	**185.5 ± 22.4**	319.1 ± 28.2	296.9 ± 8.6
MSR15018	HA – Waipoa (**awp**)	6/11	74.0	1.19	**191.1 ± 4.4**	74.0	0.72	195.8 ± 7.0	292.2 ± 8.5	196.4 ± 4.2
LP039	HA – Pukekaikiore (**apk**)	7/10	95.1	0.38	**194.7 ± 5.0**	95.1	0.40	197.7 ± 12.6	296.1 ± 11.0	192.6 ± 5.8
LP036	HA – Toatoa (**ato**)	8/10	**96.3**	**Recoil**	**205.1 ± 6.0**	100.0	7.97	208.9 ± 7.4	293.0 ± 17.7	208.8 ± 4.2
LP149	HA – Toatoa (**ato**)	4/10	67.2	1.72	**205.1 ± 6.0**	67.2	1.48	191.3 ± 23.4	311.0 ± 24.4	225.6 ± 5.0
GL2132	HA – Upper Tama (**aut**)	6/11	85.2	0.74	**209.1 ± 4.9**	85.2	0.84	211.8 ± 17.9	290.9 ± 31.0	201.9 ± 5.7
LP072	HA – Tawhairauiki (**atw**)	10/10	100.0	0.72	**217.7 ± 4.4**	100.0	0.76	219.0 ± 6.6	296.6 ± 7.2	215.6 ± 5.6
LP074	HA – Tutangatahiro (**mtu**)	6/10	89.0	0.66	**223.3 ± 5.6**	89.0	0.45	214.1 ± 16.2	305.5 ± 13.9	221.2 ± 6.6
LP113	TU	5/10	67.0	1.85	**304.4 ± 11.4**	67.0	1.06	281.1 ± 24.2	316.2 ± 41.0	336.4 ± 10.2
LP097	OT	3/11	62.2	0.51	**512.0 ± 59.4**	62.2	0.52	631.1 ± 338.4	294.6 ± 12.6	931.1 ± 57.4

[1] Formation abbreviations: OT = Otamatereinga, TU = Tupuna, MH = Mangahouhounui, HA = Haumata, TA = Taiko, MM = Mokomoko, RC = Red Crater.
[2] n/N = number (n) of heating steps used for plateau age calculation out of total (N) steps in age analysis. $\%^{39}Ar$ is the percentage of radiogenic argon released over the selected plateau steps of the total radiogenic argon. Recoil ages are noted where used instead of plateau ages: see Supplementary Materials for heating step data. $^{40}Ar/^{36}Ar_i$ = denotes the isochron intercept value. Preferred ages appear in bold typeface. Details of heating step experiments, $^{40}Ar/^{36}Ar$ intercepts, isochrons and plateau spectra are provided in the Supplementary Materials.

Table 2. Petrographic features of Tongariro eruptive formations and members in approximate stratigraphic order.

Formation	Member	Lithology	SiO_2 (wt%)[1]	MgO (wt%)[1]	Total xtals (vol%)[2]	Vesicles (vol%)	Relative phase proportions[3]	Other petrographic features[3]
Te Pupu (**TP**)	Matariki (**mmt**)	lava, pyroclastics	55.5-57.6	4.2-5.4	20-35	0-20	pl > opx > cpx > ox ~ ol	sometimes no ol and/or ox
	Toakakura (**mtk**)	lava, pyroclastics	56.9-57.6	4.0-4.9	30-35	0-10	pl > opx ~ cpx > ox > ol	sometimes no ol and/or ox
	Papamānuka (**mpa**)	lava	54.5-58.3	2.2-4.9	35-45	0-15	pl > opx > cpx > ox > ol	sometimes no ol and/or ox
Red Crater (**RC**)	Te Rongo (**mtr**)	lava, scoria, spatter	53.6-55.7	6.3-7.7	25-35	2-10	pl > cpx > ol > opx	trace ox
	Te Ahititi (**ahi**)	lava, agglutinates	59.1-60.9	3.8-4.5	25-35	0-2	pl > cpx ~ opx > ol ~ ox	-
Te Maari (**TM**)	Mangatetipua (**mgt**)	lava	~56.3	~6.9	25-30	n.d.	pl > ol ~ cpx > opx > ox	-
	Heretoa (**aht**)	agglutinates, lava	57.3-59.8	3.6-4.5	35	0-(?)5	pl > cpx > opx > ox	no ol or ap
	Paungaiti (**api**)	agglutinates, lava	58.5-60.3	3.2-4.1	25-35	0	pl > opx ~ cpx > ox	trace ap adjoined to opx-cpx-pl clots
	undifferentiated (*utm*)	lava	58.9	3.6	-	-	-	-
Makahikatoa (**MK**)	(no members)	scoria, lava	57.1-57.4	6.9-7.1	15-20	0-40	cpx ~ opx > pl ~ ol ~ ox	-
Pukeonake (**PN**)	(no members)	scoria, lava	56.0-56.9	7.9-8.9	20-35	30-35	cpx ~ pl > opx > ol > ox	-
Mokomoko (**MM**)	Te Wai Whakaata (**aww**)	lava, agglutinates	56.9-58.5	3.9-4.3	25-35	0-15	pl > cpx ~ opx > ox	trace ap adjoined to cpx-pl clots
	Mangatapate (**amt**)	lava, agglutinates	59.1-59.9	3.8-4.2	25-35	0-2	pl > opx > cpx > ox	no ol or ap
	Rangitaupahi (**ari**)	lava, spatter, agglutinates	58.6-59.9	4.4-5.1	25-40	0-40	pl > cpx > opx > ox	trace ol, trace ap adjoined to cpx-pl clots
Te Whaiau (**TW**)	-	debris flows	-	-	-	-	-	contains clasts of OT lava
(formation unclear)	undiff. Otukou lava (**uol**)	lava	~58.6	~5.9	~7	0	pl > cpx ~ opx > ol	trace hb-ox

Table 2. Continued (Taiko and Mangahouhounui formations).

Formation	Member	Lithology	SiO_2 (wt%)[1]	MgO (wt%)[1]	Total xtals (vol%)[2]	Vesicles (vol%)	Relative phase proportions[3]	Other petrographic features[3]
Taiko (**TA**)	Te Tatau (**att**)	lava, scoria, agglutinates	57.4-59.5	4.2-6.5	20-30	0-45	pl > cpx ~ opx > ox	trace ol, no ap
	Rotopaunga (**arp**)	agglutinates, lava, lapilli tuff breccias	57.6-61.3	3.0-4.2	25-35	0-15	pl > opx > cpx > ox	trace ap adjoined to cpx-pl clots
	Te Wakarikiariki (**ati**)	lava	58.9-59.1	4.0-4.6	30-35	0	pl > cpx > opx > ox	≤7 mm pl
	Te Rurunga (**atr**)	lava, scoria, agglutinates	58.1-58.3	4.9-5.0	40-45	0-20	pl > cpx > opx > ox ~ ol	-
	Waitakatorua (**awu**)	lava, bedded lapilli tuffs	56.7-59.2	4.8-5.8	30-40	0-5	pl > cpx > opx > ox	trace ol, no ap
	Otamangakau (**aok**)	lava, agglutinates	59.4-61.7	3.4-3.9	35-40	0-5	pl > opx > cpx > ox	trace ol, trace ap adjoined to opx clots
	Te Porere (**dtp**)	lava, lapilli tuffs (also as breccias), agglutinates, hyaloclastites	59.4-63.9	1.7-3.1	35-50	0-7	pl > opx > cpx > ox	trace ap in some samples
	Mangatepopo (**app**)	lava	58.6-59.5	4.2-4.9	30	0	pl > cpx > opx > ox	trace ol
	Mangahouhouiti (**mhi**)	lava, agglutinate	55.6-58.6	5.5-7.1	10-20	0-5	cpx ~ ol > pl ~ opx > ox	-
	Pungarara (**apg**)	lava	57.8-62.7	2.5-3.9	20-30	0	pl > opx > cpx > ox	trace hb-ox
	Rahuituki (**arh**)	lava	60.4-61.3	2.9-3.4	30-40	0-2	pl > cpx ~ opx > ox	no ap or ol
Manga-houhounui (**MH**)	Tātaramoa (**mtm**)	lava	~53.9	~5.3	20	25	pl > cpx > opx	trace opx and ox, no ol, ≤9 mm pl and ≤8 mm cpx
	Waiaruhairiki (**awh**)	lava, agglutinates	57.0-58.6	5.4-6.2	35-40	0	pl > cpx ~ opx > ox	≤9 mm pl and ≤8 mm cpx
	Te Pakiraki (**dpk**)	lava, agglutinates, glacial-lateral breccias	56.7-64.6	2.5-4.8	30-40	0	pl > opx > cpx > ox	trace ap in dacites and hi-SiO_2 andesites; ≤9 mm pl and ≤8 mm cpx

Table 2. Continued (Haumata, Tupuna and Otamatereinga formations).

Formation	Member	Lithology	SiO_2 (wt%)[1]	MgO (wt%)[1]	Total xtals (vol%)[2]	Vesicles (vol%)	Relative phase proportions[3]	Other petrographic features[3]
Haumata (**HA**)	Waipoa (**awp**)	lava	59.6-62.4	3.1-4.5	30-40	0	pl > cpx > opx > ox ~ hb-ox	trace serpentinised ol xenocrysts, trace ap
	Pukekaikiore (**apk**)	lava	60.0-61.5	3.6-4.2	35	0	pl > cpx > opx > hb-ox > ox	trace ol, no ap
	Toatoa (**ato**)	lava	60.1-61.6	3.4-4.6	30-35	0	pl > cpx ~ opx ~ hb-ox > ox	trace ap
	Upper Tama (**aut**)	lava, pumice, pyroclastics	59.1-63.0	2.4-2.9	30-40	0-? (PDCs)	pl > cpx > opx > hb-ox > ox	trace ap
	Tawhairauiki (**atw**)	lava	59.0-60.6	3.8-4.7	35-40	0	pl > opx ~ cpx > ox > hb-ox	trace ap
	Tutangatahiro (**mtu**)	lava	56.1-57.6	3.7-5.5	40-45	0	pl > cpx > opx > hb-ox> ox	≤6 mm cpx clots, no ap
	Lower Tama (**alt**)	lava	61.2-62.7	3.0-3.1	35	0	pl > cpx ~ opx > hb-ox > ox	-
Tupuna (**TU**)	(no members)	lava (not in-situ)	59.2-60.5	3.8-4.1	35	0	hb ~ pl > ox > cpx ~ opx	-
Otama-tereinga (**OT**)	(no members)	lava	56.0-57.0	5.3-5.4	40-45	1-7	pl > cpx > opx > ol ~ ox	ol has scythe-shaped ox + opx reaction rims

Note: major oxide abundances are normalised to 100 % anhydrous totals. Representative major oxide XRF data are presented in Table 4; full data in Supplementary Materials.

[1] XRF whole-rock major oxide data primarily from this study and Hobden (1997), but also Wahyudin (1993), Cole (1978, 1979); pre-1980 samples from Stevens and Stirling via GNS PETLAB, D. B. Townsend and G. S. Leonard pers. comm. (2016). Values are normalised to 100 % anhydrous totals.

[2] Normalised to vesicle-free basis. xtal = crystal.

[3] Abbreviations: pl = plagioclase, opx = orthopyroxene, cpx = clinopyroxene, ol = olivine, ox = Fe-Ti oxide, hb = hornblende, hb-ox = Fe-Ti oxide pseudomorphs after amphibole, ap = apatite.

Table 3. Representative major oxide (wt%) and Sr and Ba (ppm) concentrations for all map units (except undifferentiated units).

Sample	LP097	LP113	LP109	LP074	LP072	GL 2132	LP036	LP149	LP039	MSR 15018
Fm.[1]	OT	TU	HA	HA	HA	HA	HA	HA	HA	HA
Mbr.[2]	-	-	alt	mtu	atw	aut	ato	ato	apk	awp
SiO_2	55.54	59.41	62.46	56.14	59.05	61.32	60.46	59.98	60.07	59.99
TiO_2	0.68	0.54	0.43	0.66	0.57	0.56	0.59	0.62	0.61	0.65
Al_2O_3	16.66	16.91	16.97	17.82	16.23	17.30	15.60	16.47	16.39	17.10
Fe_2O_3	8.79	6.93	5.85	8.24	7.50	6.24	6.89	6.94	6.98	6.99
MnO	0.15	0.13	0.11	0.14	0.13	0.12	0.12	0.11	0.12	0.12
MgO	5.34	3.92	3.05	4.23	4.70	2.72	4.53	3.97	4.02	3.74
CaO	7.88	6.46	5.26	7.53	6.71	6.35	6.80	6.47	6.55	6.75
Na_2O	2.74	3.40	3.58	3.32	3.15	3.66	3.07	3.30	3.29	3.42
K_2O	0.80	1.04	1.13	0.89	1.17	1.45	1.40	1.30	1.30	1.28
P_2O_5	0.14	0.13	0.14	0.16	0.13	0.18	0.13	0.13	0.13	0.14
SO_3	0.04	0.01	0.04	0.04	0.04	-	0.04	0.04	0.04	0.04
LOI	0.40	0.16	0.57	-0.22	0.11	0.10	0.61	0.03	-0.04	0.19
Total	99.22	99.10	99.64	99.21	99.56	99.23	100.31	99.43	99.56	100.46
Sr	293	247	242	260	272	-	239	261	275	233
Ba	239	324	279	280	257	-	344	277	270	307

Table 3. Continued.

Sample	LP239	LP129	LP234	LP118	LP229	TG084	LP245	LP209	LP051	LP214
Fm.[1]	MH	MH	MH	MH	MH	MH	MH	MH	TA	TA
Mbr.[2]	dpk	dpk	dpk	dpk	dpk	dpk	awh	mtm	arh	arh
SiO_2	61.89	58.34	64.84	57.46	58.55	58.69	58.39	53.77	61.14	60.99
TiO_2	0.73	0.73	0.65	0.82	0.71	0.73	0.66	0.83	0.73	0.65
Al_2O_3	16.71	16.62	16.13	16.74	16.94	16.96	15.28	17.92	16.51	17.05
Fe_2O_3	6.67	8.20	5.30	8.32	7.70	7.51	7.83	9.50	7.10	6.91
MnO	0.10	0.13	0.09	0.13	0.12	0.12	0.13	0.16	0.10	0.12
MgO	3.03	3.95	2.52	4.23	4.20	3.86	5.56	5.32	2.91	3.18
CaO	5.56	6.67	4.67	6.91	6.90	7.21	7.57	7.91	5.40	5.99
Na_2O	3.27	3.02	3.30	3.04	3.15	3.23	2.87	2.72	3.27	3.28
K_2O	1.74	1.50	2.27	1.47	1.15	1.30	1.28	0.74	2.05	1.75
P_2O_5	0.17	0.16	0.17	0.17	0.15	0.14	0.14	0.15	0.18	0.14
SO_3	0.03	0.04	0.01	0.04	0.00	-	0.00	0.00	0.04	0.02
LOI	0.33	-0.06	0.37	-0.17	0.39	-0.18	-0.08	0.74	0.28	0.25
Total	100.30	99.43	100.39	99.40	100.01	99.57	99.79	99.81	99.78	100.38
Sr	189	229	200	260	222	267	357	258	222	225
Ba	366	298	435	340	255	304	251	297	343	330

Table 3. Continued.

Sample	TG077	MSR 15019	LP010	LP250	LP024	LP103	LP071	LP140	LP023	LP161
Fm.[1]	**TA**	**TA**	**TA**	**TA**	**TA**	**TA**	**TA**	**TA**	**TA**	**TA**
Mbr.[2]	**apg**	**mhi**	**amp**	**amp**	**dtp**	**dtp**	**aok**	**awu**	**atr**	**ati**
SiO_2	57.15	56.77	58.80	59.41	61.96	60.89	60.10	58.38	58.39	57.78
TiO_2	0.88	0.68	0.76	0.76	0.92	0.94	0.77	0.68	0.75	0.68
Al_2O_3	17.72	15.54	16.49	15.49	16.75	16.93	16.55	15.98	16.18	16.94
Fe_2O_3	7.90	7.82	7.78	8.19	7.43	7.73	7.21	7.30	7.99	7.72
MnO	0.13	0.14	0.13	0.13	0.12	0.12	0.12	0.12	0.13	0.13
MgO	3.29	6.31	4.23	4.88	2.01	1.97	3.44	5.12	4.89	4.44
CaO	6.93	8.14	6.95	6.40	5.32	4.91	5.92	6.90	7.13	7.56
Na_2O	3.53	2.76	3.22	3.09	3.74	3.54	3.27	3.10	3.10	3.13
K_2O	1.28	0.99	1.51	1.56	1.94	1.94	1.84	1.41	1.43	1.16
P_2O_5	0.17	0.13	0.15	0.15	0.18	0.19	0.17	0.15	0.14	0.14
SO_3	-	-	0.04	0.00	0.04	0.04	0.05	0.04	0.04	0.00
LOI	-0.12	0.86	0.30	-0.04	0.14	0.24	0.00	0.10	0.14	0.12
Total	98.86	100.18	100.42	100.13	100.61	99.51	99.53	99.38	100.37	99.84
Sr	313	363*	259	226	236	260	262	348	246	223
Ba	310	226*	337	303	418	434	395	310	272	225

Table 3. Continued.

Sample	LP211	GL 2223	LP247	LP249	LP062	LP063	LP151	LP147	LP001	TG152
Fm.[1]	**TA**	**TA**	**TA**	**TA**	**-**	**MM**	**MM**	**MM**	**PN**	**MK**
Mbr.[2]	**arp**	**att**	**att**	**att**	**uol**	**ari**	**amt**	**aww**	**-**	**-**
SiO_2	61.03	57.90	58.37	56.25	58.33	58.58	59.88	57.57	55.35	56.89
TiO_2	0.76	0.79	0.67	0.66	0.66	0.72	0.74	0.82	0.68	0.57
Al_2O_3	16.44	16.71	15.24	15.68	14.99	15.88	16.20	17.15	14.23	14.59
Fe_2O_3	7.50	7.65	7.88	8.26	7.48	7.62	7.53	8.17	7.60	7.93
MnO	0.13	0.12	0.13	0.14	0.12	0.13	0.13	0.14	0.12	0.13
MgO	3.34	4.60	5.58	6.56	5.91	4.71	4.21	4.04	9.47	7.02
CaO	5.94	7.40	7.55	7.23	7.53	6.83	6.47	7.13	7.22	9.18
Na_2O	3.27	3.23	2.88	2.44	2.99	3.08	3.16	3.04	2.64	2.37
K_2O	1.76	1.33	1.29	1.12	1.24	1.49	1.55	1.38	1.30	0.89
P_2O_5	0.16	0.17	0.14	0.14	0.15	0.16	0.16	0.17	0.14	0.08
SO_3	0.01	-	0.00	0.11	0.04	0.05	0.01	0.04	0.04	-
LOI	-0.15	0.96	-0.12	1.55	-0.25	0.01	-0.07	-0.14	1.27	-0.47
Total	100.40	100.97	99.80	100.20	99.51	99.32	100.10	99.69	100.15	99.18
Sr	233	319	358	314	386	260	252	257	264	634
Ba	423	266	244	222	250	337	351	329	297	198

Table 3. Continued.

Sample	LP003	24269	24266	TG088	TG112	TG266	TG017	TG039
Fm.[1]	TM	TM	TM	RC	RC	TP	TP	TP
Mbr.[2]	api	aht	mgt	ahi	mtr	mpa	mtk	mmt
SiO_2	59.52	56.57	56.19	59.39	53.38	54.87	55.30	54.80
TiO_2	0.74	0.75	0.71	0.73	0.72	1.05	0.87	0.75
Al_2O_3	16.21	17.37	15.86	16.54	15.45	17.60	18.13	16.61
Fe_2O_3	7.53	7.31	7.65	7.31	9.70	9.18	9.50	8.82
MnO	0.12	0.14	0.15	0.12	0.16	0.16	0.16	0.15
MgO	3.97	4.47	6.86	4.37	7.71	4.52	3.89	5.32
CaO	6.33	7.55	8.05	7.29	10.49	8.03	8.51	8.26
Na_2O	3.20	3.12	2.85	3.16	2.43	3.40	3.11	2.79
K_2O	1.64	1.16	1.29	1.48	0.63	1.08	0.94	1.09
P_2O_5	0.17	0.08	0.13	0.14	0.13	0.20	0.14	0.14
SO_3	0.04	-	-	-	-	-	-	-
LOI	-0.01	0.12	0.04	-0.54	-0.71	0.25	-1.52	-0.52
Total	99.54	98.68	99.81	99.99	100.09	100.34	99.03	98.21
Sr	301	162	155	295	278	316	214	245
Ba	322	233	233	317	134	204	166	204

All data by XRF. Full whole-rock major oxide dataset is reported in Supplementary Materials. MSR and GL samples from G. S. Leonard (pers. comm., 2016). TG samples from Hobden (1997). Samples 24269 and 24266 from Cole (1979).

*Data from solution ICP-MS (Pure, 2020).

[1] Fm. = formation. Otamatereinga (**OT**), Tupuna (**TU**), Haumata (**HA**), Mangahouhounui (**MH**), Taiko (**TA**), Mokomoko (**MM**), Pukeonake (**PN**), Makahikatoa (**MK**), Te Maari (**TM**), Red Crater (**RC**), Te Pupu (**TP**).

[2] Mbr. = member. Lower Tama (**alt**), Tutangatahiro (**mtu**), Tawhairauiki (**atw**), Upper Tama (**aut**), Toatoa (**ato**), Pukekaikiore (**apk**), Waipoa (**awp**), Te Pakiraki (**dpk**), Waiaruhairiki (**awh**), Tātaramoa (**mtm**), Rahuituki (**arh**), Pungarara (**apg**), Mangahouhouiti (**mhi**), Mangatepopo (**amp**), Te Porere (**dtp**), Otamangakau (**aok**), Waitakatorua (**awu**), Te Rurunga (**atr**), Te Wakarikiariki (**ati**), Rotopaunga (**arp**), Te Tatau (**att**), undifferentiated Otukou lava (**uol**), Rangitaupahi (**ari**), Mangatapate (**amt**), Te Wai Whakaata (**aww**), Paungaiti (**api**), Heretoa (**aht**), Mangatetipua (**mgt**), Te Ahititi (**ahi**), Te Rongo (**mtr**), Papamānuka (**mpa**), Toakakura (**mtk**), Matariki (**mmt**).

Table 4. Areas, thicknesses and volumes of edifice-forming materials on Tongariro.

Volcanic deposits						
Formation	**Package**	**Visible area (km^2)**	**'f'-factor ***	**Inferred total area (km^2) ***	**Average thickness (m)**	**Volume (km^3)**
Te Pupu (**TP**)	Matariki (**mmt**)	2.1	1	2.1	15	0.03
	undifferentiated (*utp*)	2.9	1.1	3.2	20	0.06
	Toakakura (**mtk**)	4.3	2	8.5	20	0.17
	Papamānuka (**mpa**)	4.4	3	13.1	20	0.73
Red Crater (**RC**)	Te Rongo (**mtr**)	1.1	1	1.1	50	0.05
	Te Ahititi (**ahi**)	6.6	1	6.6	80	0.53
Te Maari (**TM**)	Mangatetipua (**mgt**)	1.7	1	1.7	30	0.05
	Heretoa (**aht**)	7.2	1	7.2	50	0.36
	Paungaiti (**api**)	15.7	1.3	20.4	30	0.61
	undifferentiated (*utm*)	2.2	2	4.4	30	0.13
Makahikatoa (**MK**)	(no members)	1.4	1	1.4	40	0.06
Mokomoko (**MM**)	Te Wai Whakaata (**aww**)	1.4	1	1.4	40	0.06
	Mangatapate (**amt**)	0.3	1	0.3	30	0.01
	Rangitaupahi (**ari**)	11.5	1.1	12.6	40	0.50
Pukeonake (**PN**)	(no members)	77.5	1	77.5	10	0.77
Taiko (**TA**)	undifferentiated (*uta*)	5.5	3	16.5	15	0.25
	Te Tatau (**att**)	4.8	2	9.6	30	0.29
	Rotopaunga (**arp**)	13.8	1.5	20.7	90	1.86
	Te Wakarikiariki (**ati**)	0.3	15	4.4	50	0.22
	Te Rurunga (**atr**)	2.3	2.2	5.2	40	0.21
	Waitakatorua (**awu**)	1.2	2	2.3	130	0.30
	Otamangakau (**aok**)	16.1	1.5	24.2	60	1.45
	Te Porere (**dtp**)	16.0	2.5	40.1	50	2.00
	Mangatepopo (**amp**)	0.3	8	2.1	20	0.04
	Mangahouhouiti (**mhi**)	10.8	1.1	11.9	50	0.59
	Pungarara (**apg**)	1.0	1.3	1.3	100	0.13
	Rahuituki (**arh**)	9.1	3	27.2	40	1.09
Mangahouhounui (**MH**)	undifferentiated (*umh*)	0.1	1	0.1	60	0.01
	Tātaramoa (**mtm**)	0.1	5	0.4	20	0.01
	Waiaruhairiki (**awh**)	0.1	8	0.9	30	0.03
	Te Pakiraki (**dpk**)	1.2	7	8.5	130	1.34
Haumata (**HA**)	undifferentiated (*uha*)	0.6	1	0.6	90	0.05
	Waipoa (**awp**)	7.1	1.8	12.8	100	1.28
	Pukekaikiore (**apk**)	1.0	1.3	1.3	100	0.13
	Toatoa (**ato**)	2.4	1.5	3.6	90	0.33
	Upper Tama (**aut**)	2.1	1.5	3.2	130	0.41
	Tawhairauiki (**atw**)	12.2	1.7	20.7	60	1.24
	Tutangatahiro (**mtu**)	10.8	2	21.6	60	1.30
	Lower Tama (**alt**)	0.9	4	3.5	100	0.35
Tupuna (**TU**)	(no members)	0	-	-	-	?
Otamatereinga (**OT**)	(no members)	0.1	-	-	-	?
Total for exposed map units		**220**	**-**	**220**	**410**	**19.03**

Non-volcanic deposits					
Deposit type	**Glacial period**	**Visible area (km^2)**	**Thickness (m)**	**Volume for rectangular profile (km^3)**	**Volume with triangular profile (km^3)**
Moraines	MIS 7-5	4.9	60	0.30	0.15
	MIS 4-3	9.1	60	0.54	0.27
	MIS 2	11.5	60	0.68	0.34
Te Whaiau Fm	-	52.8	2-26 (~12)	0.63	-

* Inferred total area is the visible area multiplied by the 'f'-factor. 'f'-factor represents the proportion of buried area that connects units to their inferred source vent location, as determined by field relations.

Erosion is not accounted for. Limited outcrop of TU and OT are inadequate for estimating volumes. Volume estimation procedures are explained in the Supplementary Materials.

Table 5. Comparison of features and histories of Tongariro and Ruapehu volcanoes.

Feature	Sub-aspect	Tongariro	Ruapehu
Relative age	Oldest edifice age determination	304 ± 11 ka [$^{40}Ar/^{39}Ar$] (this study: Table 1)	205 ± 27 ka [$^{40}Ar/^{39}Ar$] (Gamble et al., 2003)
	Oldest associated material	<349 ka andesite boulders overlying Whakamaru Ignimbrite [~9 km N of edifice] (M. Rosenberg, pers. comm., 2018; Bayly and Quinlan, 1965; Downs et al., 2014) 349-309 ka Turakina Formation debris flows [~100 km S] (Tost and Cronin, 2015; Whakamaru age from Downs et al., 2014; marine terrace stratigraphy from Pillans, 1983)	180-160 ka Oreore Formation [~30 km S of Ruapehu] (Tost and Cronin, 2015)
Volcano growth history	Vent spacing*	Within ~8 km on transect	Within ~4 km on transect
	Sector collapse events that can be linked to observable collapse scars/obvious deposits	50-45 ka Te Whaiau Formation [NW flank] (Lecointre et al., 2002; Townsend et al., 2017)	~5.2 ka Mangaio Formation [SE flank] (Donoghue and Neall, 2001; age via OxCal reprocessing by Townsend et al., 2017) ~10.5 ka Murimotu Formation [NW flank] (Palmer and Neall, 1989; Eaves et al., 2016a)
	Flank and peripheral vents	40-30 ka Pukeonake Formation [6 km W of edifice] (Townsend et al., 2017) 130-96 ka Mangahouhouiti Member [within 1 km W of upper edifice] 189-130 ka Tātaramoa Member [possibly vented from Te Tatau summit, which is 2 km NE of Central Crater: cf. Fig. 2]	11.4-8.6 ka Saddle Cone Member [4 km N of edifice] (Hitchcock and Cole, 2007; Conway et al., 2016; Greve et al., 2016; Townsend et al., 2017) undifferentiated spatter cone near State Highway 1 [14 km E of edifice: E1835957 N5648515 elev. 1082 m (NZTM2000)] (B. M. Kennedy, pers. comm., 2016; Townsend et al., 2017)
	Total number of vents	14 effusive vents (this study) + 3 Holocene explosive-only vents (Topping, 1973; Nairn et al., 1998) [compares with 16 effusive vents + 3 Holocene explosive-only vents in Hobden (1997)]	At least 5, with older vent areas reactivated after 5-100 kyr hiatuses (Conway et al., 2016)
Glacial history	Moraine distribution	Not known on N north flank	On all flanks
	Moraine ages	MIS 7-2 [~220-18 ka] (Eaves et al., 2016a; Townsend et al., 2017; Cole et al., 2018) MIS 7-5 moraines more common than on Ruapehu (labelled t6 in Townsend et al., 2017)	MIS 6-1 [~200-5 ka] (Conway et al., 2016; Townsend et al., 2017) MIS 6-5 moraines only on NW flank. MIS 2-1 much more abundant than on Tongariro (labelled t2 and t1 in Townsend et al., 2017)
Volumes	Total edifice	~90 km^3 (see section 4)	~150 km^3 (Gamble et al., 2003; Conway et al., 2016)
	Effusive (Holocene)	~2.0 km^3 (see section 5.5)	~9.6 km^3 (Conway et al., 2016)
	Explosive (Holocene)	~6.2 km^3 (see section 5.5)	~1.5 km^3 (see section 5.6)

* Refers to all inferred previous and all presently visible vent foci referenced to an upper-edifice transect in NNE direction, parallel to the TVZ arc axis.

Fig. 1. Hill-shaded digital surface model (DSM) highlighting the intermediate-composition volcanoes that dominate the southern TVZ, which are each labelled. Red lines indicate traces of faults that were active during the Quaternary, following Townsend et al. (2017). Map projections are the New Zealand Transverse Mercator 2000 (NZTM2000) in eastings and northings and WGS84 Mercator in decimal degrees. The 2 m-resolution DSM was developed by GNS Science from photogrammetry of aerial photos obtained in 2010 and 2012 (see Gómez-Vasconcelos et al., 2016, for details). Bottom-right inset shows the position of the map area (red box) in New Zealand's North Island. The boundary between the continental crust (CC) and oceanic crust (OC) is after Gamble et al. (1993). Dashed-line inset indicates the area shown in Fig. 2.

Fig. 2. Major landmarks on and around Tongariro volcano. Water bodies are shaded blue. BL = Blue Lake, CC = Central Crater, LR = Lake Rotoaira, LM = Lower Te Maari Crater, LT = Lower Tama lake, NC = North Crater, NG = Ngauruhoe, P = Pukeonake, PK = Pukekaikiore, R = Rotopaunga summit, RC = Red Crater, TS = Tongariro summit, TT = Te Tatau summit, SC = South 'Crater' Cirque (e.g. Cole et al., 2018), UM = Upper Te Maari Crater, UT = Upper Tama lake. The location of Ketetahi Hot Springs (HS) is shown more precisely in Fig. 9.

Fig. 3. Space-time relationships of map units (not a stratigraphic log). 'Age' boundaries show adopted age ranges for map units but do not indicate continuous activity during these intervals. Bold black lines indicate observed field contacts; dashed bold lines indicate adjacent and inferred contacts. Horizontal positioning and width of each box shows the approximate distribution across N-E-S-W sectors, but does not indicate runout distance. Grey dashed lines show key time horizons of regional rhyolitic tephra from central TVZ volcanoes (≥50 km to north): see text and Supplementary Materials for discussion of their imposed age control on Tongariro units. Question marks indicate poorly constrained age boundaries. Note the time break (~450-350 ka) and change in scale (~235 ka). Formation and member abbreviations are as in Table 2. Members are grouped by their parent formations as indicated by grey boxes in the background. An inset map shows N-E-S-W directions and the approximate positions of each formation (abbreviated) except the Taiko Formation (TA). $^{40}Ar/^{39}Ar$ age determinations and 2 s.d. uncertainties are symbolised with white circles and error bars; one K/Ar age determination from Hobden et al. (1996) is shown for unit *alt* with a yellow square with error bars. Mean values for $^{40}Ar/^{39}Ar$ age determinations on *awh* (LP245) and *dpk* (LP118) indicate stratigraphic ordering that is opposite to field relations: arrows

emanate from the field positions of these samples and point to their respective age symbols.

Fig. 4. Distribution of eruptive units on Tongariro ranging in age from ~0.5 Ma to 189 ka. Unit abbreviations as in Table 2. Key landmarks mentioned in the text are labelled. See Table 1 for $^{40}Ar/^{39}Ar$ age results and Table S5.1 in the Supplementary Materials for a summary of K/Ar (Hobden et al., 1996) and $^{40}Ar/^{39}Ar$ age results for each unit.

Fig. 5. View of southern Tongariro, looking ENE, showing relationships between members of the Haumata and Te Pupu formations. Unit abbreviations as in Table 2. Annotations show locations of samples with determined $^{40}Ar/^{39}Ar$ ages as in Table 1.

Fig. 6. View of western Tongariro, looking E from the Pukeonake cone, showing relationships between members of the Haumata, Taiko, Mokomoko, Makahikatoa and Te Pupu formations. Unit abbreviations as in Table 2. Annotations show locations of samples with determined $^{40}Ar/^{39}Ar$ ages as in Table 1. Mangatepopo Hut = M. Hut.

Fig. 7. Lava-ice interaction features on Tongariro. **(a)** Alternating layers of intercalated coherent lava and monomict breccia deposits composed of subangular lava fragments in Te Pakiraki Member lava with an inferred age between 150-130 ka at this locality, northern Mangahouhounui valley (E1832474, N5665970, 1580 m a.s.l.). Geologist circled in red is 1.8 m tall. **(b)** Horizontal column joints in Te Pakiraki Member lava with an inferred age between 150-130 ka at this locality, southern Mangahouhounui valley (E1831657, N5664737, 1610 m a.s.l.). Column diameters are between 10-25 cm. Sledgehammer handle (red) is 1 m. **(c)** Layers of lapilli tuff breccia (5-70 cm thick) intercalated with layers of fine sediment (grain sizes <<1 cm, layers 1-10 cm thick) and coherent lavas (≥60 cm thick) in Waitakatorua Member ridge-top deposits between the Oturere and Mangahouhounui valleys (E1831362, N5664691, 1680 m a.s.l.).

Fig. 8. Distribution of the Taiko Formation (TA) eruptives for the interval between 133 to 52 ka. The source of the undifferentiated Otukou lava (uol) is unclear. Unit abbreviations as in Table 2. Key landmarks are labelled. $^{40}Ar/^{39}Ar$ age determinations on LP051 and LP126 were adversely affected by groundmass glass but are indicated here because heating step results are provided in the Supplementary Materials for these samples. $^{40}Ar/^{39}Ar$ age results are presented in Table 1 and summarised with K/Ar age results (Hobden et al., 1996) in Table S5.1 of the Supplementary Materials for each stratigraphic unit.

Fig. 9. Aerial view of eastern and upper Tongariro, looking W, showing relationships between members of the Haumata, Mangahouhounui, Taiko, Mokomoko, Te Maari and Red

Crater formations. Unit abbreviations as in Table 2. Annotations show locations of samples with determined $^{40}Ar/^{39}Ar$ ages. (GNS VML ID 6742, courtesy of B. Scott.)

Fig. 10. The distribution of Pukeonake (PN), Mokomoko (MM) and Te Whaiau (TW) formations. PN was vented from one or more satellite cones, shown by triangles, with the main cone as the largest triangle. PN lavas overlie the TW debris deposits. Rangitaupahi (ari) and Mangatapate (amt) members were erupted from North Crater (NC) vents. The Te Wai Whakaata Member (aww) was erupted from a vent at the present-day location of Blue Lake (BL). Field relationships indicate that, at the time the North Crater and Blue Lake vents were growing, Central Crater (CC) was filling with reworked erupted material. Key landmarks are labelled. See Table 1 for $^{40}Ar/^{39}Ar$ age results. LP001 is indicated without an age value because $^{40}Ar/^{39}Ar$ age analysis was adversely affected by groundmass glass, but heating step results are presented in the Supplementary Materials. South Cirque (SC) and Red Crater (RC) are annotated.

Fig. 11. Distribution of the Makahikatoa, Te Maari, Red Crater and Te Pupu (Ngauruhoe) formations. Identical colours reflect similar ages of these contemporaneously active but separate vent systems. Age relationships are largely determined from tephrostratigraphy, as explained in section S5 in the Supplementary Materials. $^{40}Ar/^{39}Ar$ age determination data for TG088 are provided in Table 1. Key landmarks are labelled.

Fig. 12. Comparisons between K/Ar and $^{40}Ar/^{39}Ar$ age determinations for the same map units (e.g. Table S5.1 in the Supplementary Materials), coloured by K/Ar sample groundmass (GM) texture: red (holocrystalline) and blue (glass-bearing). $^{40}Ar/^{39}Ar$ ages are total gas and weighted mean plateau ages (WPMA) as indicated. Source $^{40}Ar/^{39}Ar$ data in Table 1. LP039 and GL2007 $^{40}Ar/^{39}Ar$ ages are used for comparisons against K/Ar ages for the Toatoa and Rotopaunga members because other $^{40}Ar/^{39}Ar$ ages in these members are recoil and isochron values, respectively (Table 1). Whole-rock K_2O concentrations are from Hobden et al. (1996). Crystal percentages and groundmass textures from Hobden (1997) and this study (Table 2). **(a)** Total gas $^{40}Ar/^{39}Ar$ age determinations vs. K/Ar age determinations by Stipp (1969) and Hobden et al. (1996): errors are 2 s.d. **(b)** Whole-rock K_2O concentrations in K/Ar samples vs. the difference between total gas $^{40}Ar/^{39}Ar$ ages and K/Ar ages (positive value = older $^{40}Ar/^{39}Ar$ age). Reference sample (LP113) with an inaccurate total gas $^{40}Ar/^{39}Ar$ age is annotated for two K/Ar comparisons (TG136 – Hobden et al., 1996; 3254 – Stipp, 1969). **(c)** Whole-rock K_2O concentrations in K/Ar samples vs. the difference between preferred $^{40}Ar/^{39}Ar$ ages (either WMPA or isochron ages) and K/Ar ages (positive value = older

$^{40}Ar/^{39}Ar$ age). Exceptions for (b, c): K_2O concentrations used for comparisons with Stipp (1969) K/Ar results are from this study: 3254 (LP113) and 3258 (LP062). **(d)** The difference between preferred $^{40}Ar/^{39}Ar$ ages and K/Ar ages (either WMPA or isochron ages, as in (c) vs. the concentrations of crystals in whole-rock K/Ar samples.

Fig. 13. CI chondrite-normalised rare earth element (REE) concentrations for hornblende-phyric andesite boulders in the Turakina Formation debris flows (Tost et al., 2016) compared with Tongariro's Tupuna Formation and Lower Tama Member (Haumata Formation), which are hornblende-phyric and contain pseudomorphs after amphibole, respectively. REE concentrations in Ruapehu's clinopyroxene-dominant Te Herenga Formation (Conway et al., 2018) are shown for comparison. Tongariro trace element data are from Pure (2020) and Hobden (1997: those samples with incomplete REEs [TG136, TG292]). All compositional fields for Tongariro, Ruapehu and Turakina materials are indistinguishable within analytical uncertainty. CI chondrite normalisation uses the values of McDonough and Sun (1995).

Fig. 14. Vent age comparison against vent lifespan at Tongariro. Formations and members are organised into groups with continuously sustained vent position with new boxes reflecting vent position shifts. Vents are grouped into distinct clusters within 1 km^2 and labelled here by formation: Tupuna (TU), Haumata (HA) which includes the Waipoa Member (awp), Mangahouhounui (MH), Taiko (TA), Mokomoko (MM: North Crater and Blue Lake vents), Pukeonake (PN), Te Maari (TM), Makahikatoa (MK), Red Crater (RC) and Te Pupu (TP: Ngauruhoe is the vent).

Fig. 15. Sedimentary deposits on Tongariro and part of its ring plain, and the preserved distribution of the 1.8 ka Taupō ignimbrite. Note the small remnant above 1800 m a.s.l. on North Crater's summit (labelled). Moraines, glacial outwash fans and swamp areas are also indicated. MIS = Marine Isotope Stage. Geology adapted from Eaves et al. (2016a) and Townsend et al. (2017).

Fig 16. **(a)** Valley ice thicknesses inferred from geologic features. Note the shift in eruptive focus at ~193 ka from S to N (dashed line). The key states the maximum elevation (in m a.s.l.) of outcrops used to infer ice thicknesses, which are based on average thicknesses in Table 4. Ice thicknesses inferred from moraines (1370-1480 m a.s.l.) were dated with cosmogenic ^{3}He are by Eaves et al. (2016a). The dark blue-shaded period is New Zealand's Last Glacial Maximum (NZ LGM) (Williams et al., 2015). Plotted data are reported in Supplementary Materials S8. **(b)** Benthic $\delta^{18}O$ record and Marine Isotope Stage (MIS) intervals after Lisiecki and Raymo (2005). Light blue-shaded

periods reflect major periods of ice coverage on Tongariro; the dark blue-shaded period is New Zealand's Last Glacial Maximum (Williams et al., 2015). **(c)** Cumulative volumes of map units. Width of crosses reflects the adopted age range of each unit (section 3.2). One is exception is the Te Pakiraki Member (dpk) which is subdivided into pre- and post-151 ka (Waiaruhairiki Member) ages. Undifferentiated units and Tupuna and Otamatereinga formations are not shown. Red and blue lines are regressions calculated from midpoints of adopted age ranges (section 3.2) and average volumes (Table 4) for five intervals of distinct edifice-building rates, which correspond to warm and cool climatic periods, respectively. **(d)** Time-composition systematics for SiO_2 concentrations in each stratigraphic unit (whole-rock samples), shown as crosses. Te Pakiraki Member subdivided as in (a). Cross heights represent the range of mean values for all samples of that unit. Red symbols are flank vents: 189-130 ka Tātaramoa Member (mtm), 40-30 ka Pukeonake Formation (PN), ~17.5 ka Makahikatoa Formation (MK). See data in Tables 2 and 3. **(e)** Time-composition systematics for MgO concentrations in all stratigraphic units, symbolised as in (d). Regression lines (light grey) calculated between interpreted vertices A_1-A_9 have r^2 values generally between 0.50-0.98 (see Supplementary Materials section S7). Faint lines projected from (e) to (b, d) show the positions of A_1-A_9 vertices and the Mangahouhouiti Member (mti) and PN and MK.

CRediT authorship contribution statement

L.R. Pure: Conceptualization, Methodology, Formal analysis, Investigation, Resources, Data curation, Writing - original draft, Writing - review & editing. **D.B. Townsend**: Conceptualization, Methodology, Investigation, Supervision, Writing - review & editing. **G.S. Leonard**: Conceptualization, Methodology, Investigation, Supervision, Writing - review & editing. **C.J.N. Wilson**: Visualization, Project administration, Funding acquisition, Supervision, Writing - review & editing. **A.T. Calvert**: Methodology, Investigation, Writing - review & editing. **R.P. Cole**: Investigation, Writing - review & editing. **C.E. Conway**: Conceptualization, Writing - review & editing. **J.A. Gamble**: Conceptualization, Investigation, Supervision, Writing - review & editing. **T.'B'. Smith**: Supervision, Writing - review & editing.

Declaration of interests

☒ The authors declare that they have no known competing financial interests or personal relationships that could have appeared to influence the work reported in this paper.

☐The authors declare the following financial interests/personal relationships which may be considered as potential competing interests:

Highlights

- We present new $^{40}Ar/^{39}Ar$ ages for Tongariro volcano to reconstruct the edifice growth history from ~310 ka
- Growth of the volcano occurred concurrently with at least two glacial periods and lava-ice interactions
- Growth rates of the volcano differ between glacial and interglacial periods (by a factor of ~5) due to preservation biases
- Magmatic compositional cycles were not tied to glacial-interglacial cycles
- Irregular cyclicity in MgO concentrations is observed on ~10-70 kyr intervals which represent volcano-wide mafic replenishment episodes
- Multiple vent foci were active simultaneously and sequentially through the last ~200 ka of activity